Phase control experiments utilizing the second harmonic field and applications in the excitation of an autoionizing state and control of decay to multiple continua

Master Thesis

Submitted by:

E. M. Papastathopoulos

University of Crete
Heraklion

Physics Department

Microelectronics and Optoelectronics
Postgraduate studies program

Supervisor: Prof. D. Charalambidis

June 2001

.

Dedicated to :

Aspasia Fragouli.

.

Relevant Publications

1. E. Papastathopoulos, D. Xenakis and D. Charalambidis
   Phys. Rev. A **59** 4840 (1999)

2. E. Papastathopoulos, E. Hertz, N. A. Papadogiannis, Th. Kitsopoulos, A. Saenz and P. Lambropoulos (submitted)

3. "Quantum Control in atomic systems", D. Charalambidis, N. E. Karapanagioti, D. Xenakis, E. Papastathopoulos, O. Faucher, E. Hertz, S. Cavalieri, R. Eramo, L. Fini and M. Materazzi Proc. Of the *International Workshop on Coherent Control in Atoms, Molocules and Semiconductors* Kluwer Academic Publ, Eds. Walter Potz and A. Schroeder p. 15-26, 1998.

Presentations in Conferences – Meetings

1. " Recent experiments of quantum coherent control in atomic systems ", *international Workshop on Coherent Control of Carrier Dynamics in Semiconductors*, Chicago, May 1998. (Presented by Prof. D. Charalambidis as invited speaker)

2. " Recent experiments in quantum control in atoms" 9th *Intern. Symposium on Resonance Ionization Spectroscopy and its applications*". (RIS98), Manchester, June 1998. (Presented by Prof. D. Charalambidis as invited speaker)

3. " Quantum control in atomic and molecular systems " *Sixth Symposium on Laser Spectroscopy*, KAERI, Korea, 3-4 November 1998. (Presented by Prof. D. Charalambidis as invited speaker)

4. *Gordon Research Conference on Quantum Control of Atomic and Molecular motion*, Plymouth State College in Plymouth, NH, 1-6 August 1999. (poster presentation by E. Papastathopoulos)

5. *COCOMO Scientific Workshop 2001*, Imperial College London, 23 – 24 April 2001. (Presented by E. Papastathopoulos)

.

List of Figures

.

.

List of tables

.

Contents

.

.

.

1.   Introduction

The concept of coherent control was initially motivated by the idea of controlling the products of a chemical reaction utilizing the coherent properties of laser light. Pioneer approaches on this issue are met in the literature and are usually categorized as one in the time domain and the other in the frequency domain. The time domain approach (pump-probe), introduced by Tannor & Rice [1], utilizes a sequence of ultrashort light pulses to create and probe a wave packet (WP) of molecular eigenstates. Experimental demonstration of this method came from Baumert & Gerber [2] in the control of Na dimmer excitation. The frequency domain approach (phase control) was developed by Brumer & Shapiro [3] one variation of which is the subject of the present work. In multi photon excitation due to the large number of photons involved, coupling between initial and final states of the quantum system can be achieved with more than one combination of photons. The result is a quantum mechanical interference between the competing excitation paths, and may be thought of as a quantum mechanical analogue of Young's two-slit experiment. Details of the formulation of this method are presented in Appendix A. The first experimental demonstration of this method came from Chen Ce and Elliott [4] which is discussed to more extent in a later paragraph. Besides controlling the products of chemical reactions, the key idea of interference between two independent

.

quantum channels that connect the same initial and final states of a quantum system has led to extensive experimental and theoretical studies of what has now been established as phase-sensitive coherent control. The ability to drive a molecular or atomic system is proved a valuable tool in the study of laser-molecule and laser-atom interaction. Coherent control methods are applied extensively in manipulating excitation processes and ionization rates, ionization and dissociation branching ratios, autoionization line shapes, angular distributions of photo absorption products as well as harmonic generation [5–18]. From the above we notice the experimental work by Gordon and co-workers [9] who excited a beam of DI molecules [10] with one photon of 117.90 nm and three photons of 353.69 nm. The excited molecules decayed either by autoionization to produce DI$^+$ or by predissociation to produce a ground state D atom and an electronically excited I atom. In the second case the I atom can absorb additional photons to produce I$^+$. As the phase difference between the two laser beams was increased, the ion signals varied sinusoidally (figure 1.1). The most important point is that the two oscillating ion signals differ one from another by a constant phase lag $\Delta\delta$ so that the ratio of I$^+$ to DI$^+$ could be controlled by varying the phase difference between the two laser beams. Further investigation by Gordon et.al. [10] reveals the dependence of the phase lag on the final state energy, associating the effect to the presence of a molecular autoionizing state namely the $5s\sigma$ resonance. Further theoretical investigation [19-20] on the origin of the phase lag verify that the general condition for non

12

.

zero phase lag is that the multiple continua, in which the system decays, to be coupled, and is this role that the autoionizing resonance plays in the experiments by Gordon group.
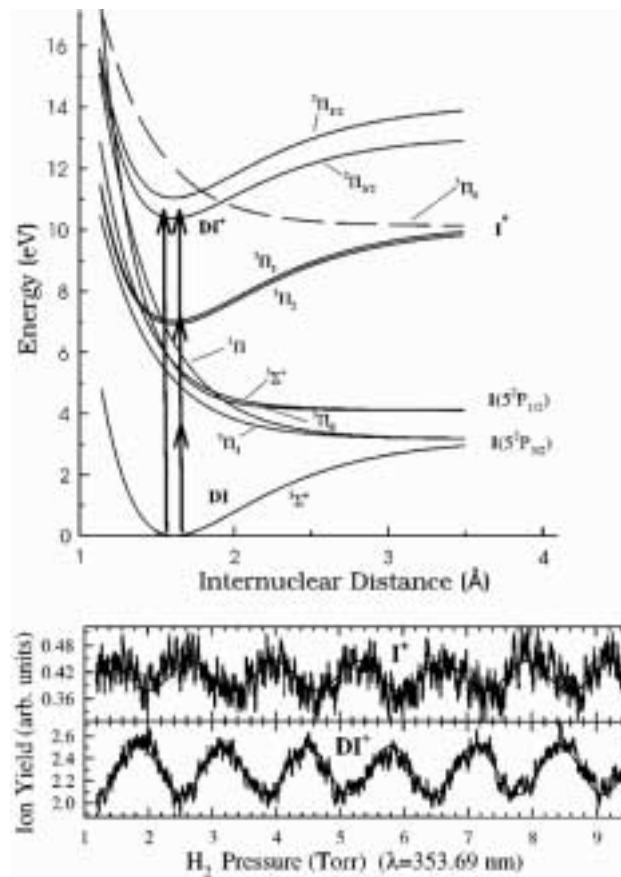
Fig.1.1 Control of the predissociation and autoionization of DI by quantum path interference [17].

.

Our experiment work is focused on phase control schemes where the final state lies in the vicinity of an atomic autoionizing resonance justifying the title of this essay. More specifically our motivation origins from the theoretical calculations by T. Nakajima and P. Lambropoulos [11-12] applying the idea of phase control scheme to control the excitation of an autoionizing state and the Fano profile [21-22] of this autoionizing resonance (see also Appendix B). Figure (1.2) summarizes some aspects of this theoretical work for the general case of a discrete state embedded in single continuum. Consider the transition to this autoionizing resonance with both a three photon and a one transition using two phase correlated laser fields, the fundamental and the third harmonic field. By varying the relative phase of the fields it is apparent that the line shape of the resonance changes (figure 1.2). Different figures represent different intensities of the laser field, while the ratio of the quantum amplitudes of the two channels remains constant. Further discussion on the intensity dependence of the line shape is met in a later paragraph. Based on the asymmetry properties of the line shape it is deduced that by varying the relative phase of the excitation fields the discreet or the continuum parts of the autoionizing resonance can be selectively enhanced or cancelled. On the same reference one finds application in a real

14

.

atomic system, namely the Xe atom where the control of the branching ration of the ionisation to the $P_{1/2}$ and $P_{3/2}$ thresholds is demonstrated in a 3+1 control scheme. In this case the coupling between the two continua is achieved via the autoionizing resonances $[P_{1/2}]8s_{1/2}(J=1)$, $[P_{1/2}]6d_{3/2}(J=1)$ and $[P_{1/2}]6d_{5/2}(J=3)$. These resonances are depicted in figure 1.3 where the notation is changed to 8s', $6d_1$' and $6d_3$' respectively. In the later graph the ionization rate is calculated as a function of the final state energy for different values of the relative phase, as well as for incoherent excitation.

The structure of this essay is as follows: First the interference schemes under investigation are presented. Then the experimental set-ups are fully discussed before presenting the sequence of experiments conducted. Finally based on our experimental results several aspects, both experimental and theoretical, are discussed while the essay closes with perspectives of this experimental investigation. Special care is also given to the several appendixes, the aim of which is to clarify several aspects and formulation to the reader not familiar with the special subject of phase control and autoionization.

.
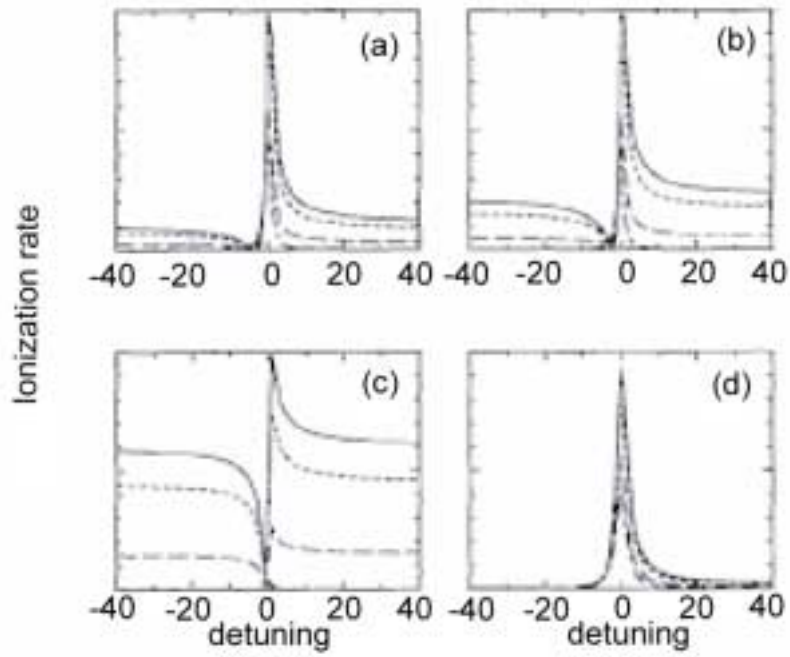
Fig. 1.2 Variation of the phase-dependent line shape. Different lines refer to different phases (φ=0 solid line, $\pi/3$ dotted, $2\pi/3$ dashed and π dot-dashed) while different figures refer to different intensities [12].

.
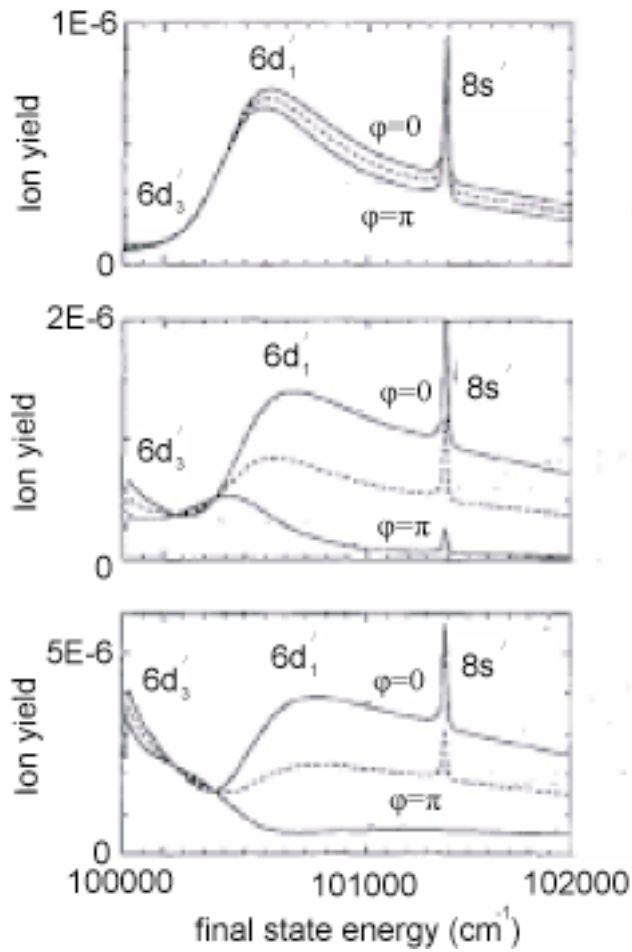
Fig. 1.3 Change of autoionization line shapes in Xe through the relative phase of two laser fields. The dashed line represents incoherent ionisation while the solid lines refer to different phases 0 and π as indicated on the figure. The three different graphs are calculations at different laser intensities [12].

2.   Investigated Schemes

.

2.1   Scheme 1. (REMPI in Xe)

The first excitation scheme in which we demonstrated   phase-sensitive ionization concerns Xe atoms. It involves absorption of photons of the fundamental and the second harmonic fields, that couple the ground state of Xe $5p^6$ to the bound $6p$ [3/2]$_2$ excited state of Xe. This state is reached via (i) four-photon absorption of the fundamental and (ii) two-photon absorption of the second harmonic. The atom are then ionised absorbing one more photon of the fundamental field. The excitation scheme is depicted in Fig. (2.1). The multi photon ionisation via a bound resonance, as in the above scheme, is known from the literature as resonant multi-photon ionisation (REMPI).   The wavelength of the fundamental is tuned to 504.97 nm and consequently the second harmonic field is at 252,48nm which lies in the UV region. The excitation is exactly on resonance with the $6p$ [3/2]$_2$ state while the virtual intermediate state excited with three fundamental photons is strongly affected by the presence of the bound $6s$ [3/2]$_1$ state (about 8636,2cm^{-1} detuning).

The excitation probability of the $6p$ [3/2]$_2$ state in this case is given by:

$$W \propto \left[\mu^{(4)}E_{10}^4\right]^2 + \left[\mu^{(2)}E_{20}^2\right]^2 + 2\mu^{(4)}\mu^{(2)}E_{10}^4E_{20}^2 \times \cos\left[2(\vartheta_2 - 2\vartheta_1)\right] \quad (2.1)$$

where the indices i =1,2 refer to the fundamental and the second harmonic field. $\mu^{(n)}$ is the effective n-photon (four visible and two UV) electric dipole moment of the transition between the ground state and the resonant state, while E_{i0} is the

19

.

electric-field amplitude of the laser beams. For the derivation of the later equation can be found in Appendix A. Hence, the probability can be controlled through the phase difference $\Delta\vartheta=2(\vartheta_2-2\vartheta_1)$. This excitation probability is probed through the one photon ionisation from the $6p$ $[3/2]_2$ state. The phase of the last probe to the continuum photon does not take part in the interference because it is common for both excitation channels.
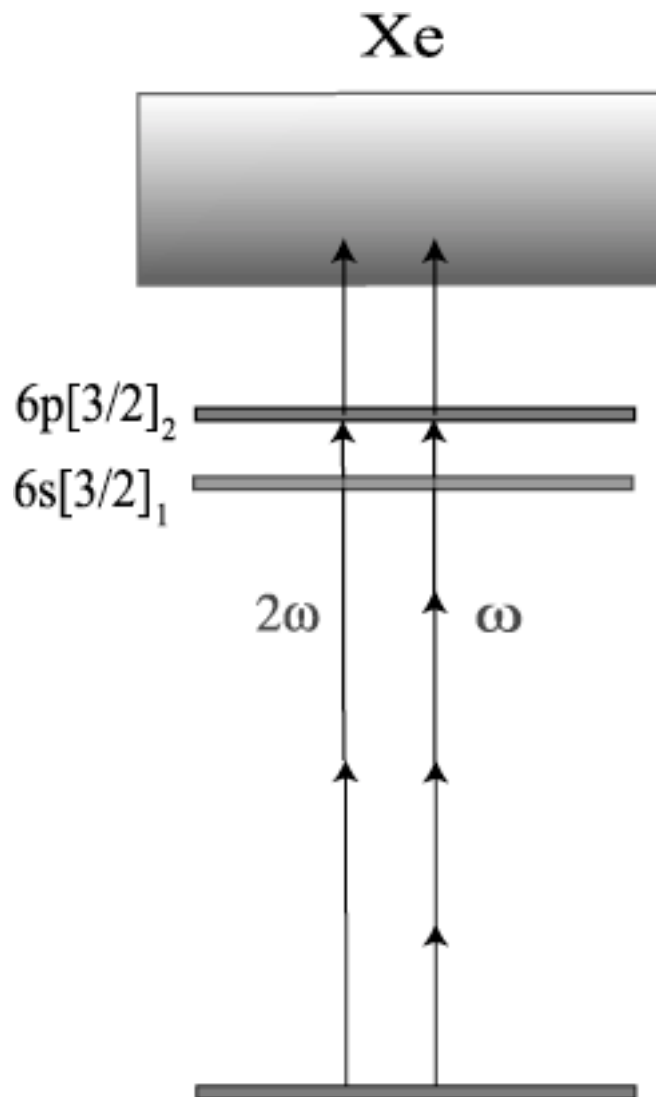
Fig.2.1 Excitation scheme 1.

.

Scheme 2. (AIS in Mg)

In the second scheme investigated the final state is in the continuum of the atom, which in this case is the Mg atom and is reached via a four photon transition (of the fundamental), (or with 2 photons of the second harmonic). It lies energetically in the vicinity of an autoionization resonance, namely the $3p^2$ ^1S state. This state has been studied extensively both theoretically [23] and experimentally [24], and lies 68785cm^{-1} above the ionization threshold of the Mg atom. The width of the states is about 200cm^{-1} due to it's short lifetime in the femto second regime.

In order to get an insight into the excitation process, the two valence electrons of Mg which populate the 3s ground orbital are both excited to the $3p$ orbital, then due to coulombic repulsion (configuration interaction CI) one of the electrons is forced out of the atom while the second electron returns to the $3s$ ground state. Doubly excited states as $3p^2$ are often described as discrete states embedded in the continuum of the atom and their wave function is expressed in terms of a discreet and a continuum part (see Appendix B). This results in asymmetric profile of the doubly excited resonance. In the low intensity regime the lifetime and therefore the width of the resonance depends only on the strength of configuration interaction.

.

Formulation of the autoionizing state (AIS) wavefunction was originally introduced by U. Fano [25] as:

$$\left|\Psi_E\right\rangle = \frac{\sin\Delta(E)}{\pi V_E}\left|\Phi_E\right\rangle - \cos\Delta(E)\left|c\right\rangle \tag{2.2}$$

where

$$\left|\Phi_E\right\rangle = \left|a\right\rangle + P\int dE_c \frac{V_{ca}(E_c)}{E - E_c}\left|c\right\rangle \tag{2.3}$$

is the bound state $\left|a\right\rangle$ modified by the CI coupling to $\left|c\right\rangle$. The bound part $\left|a\right\rangle$ is generally dominant in the expression of $\left|\Phi_E\right\rangle$ thus the later is usually referred to as the bound part of the AIS wave function. Thus $\left|\Psi_E\right\rangle$ is a linear combination of a bound and a continuum component. Details of the derivation of the above expressions are presented in Appendix B.

For a complete review the reader is also referred to the work by P.Lambropoulos [26] where the excitation of AIS in strong laser fields as well as schemes of coupled AIS's are studied theoretically.

In the presence of the two color laser field ($\omega,2\omega$) one can describe the excitation process as the interference of two channels, each of which is itself the result of interfering excitation pathways, one coupling the ground state $\left|g\right\rangle$ to the continuum $\left|c\right\rangle$, and the other coupling $\left|g\right\rangle$ to the bound $\left|\Phi_E\right\rangle$ which then decays to the continuum (fig. 2.2).

.

In the investigated scheme an analytical expression of the total ionization rate is not possible, one has to solve the Liouville equation of the density matrix of the system in order to meet quantitative results for the excitation probabilities and also take into account all the intermediate virtual states of the multi photon excitations. As mentioned in the introduction numerical, simulations on similar schemes have been examined theoreticaly by T. Nakajima and P. Lambropoulos [12].
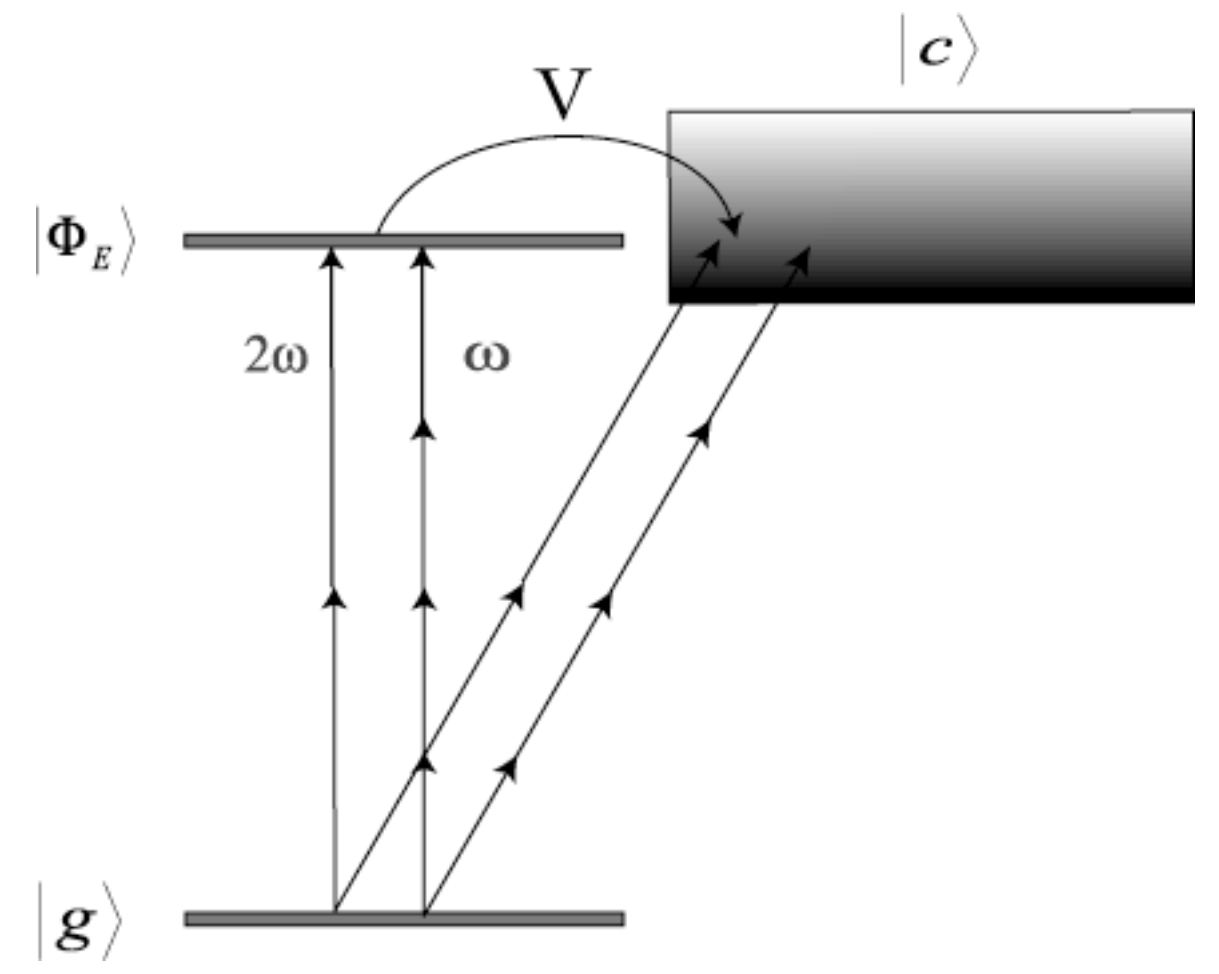
Fig. 2.2 Interference scheme in AIS

.

2.3   *Scheme 3.   (Two continua in Xe).*

In the third scheme investigated the final state in the continuum of the Xe atom is reached via a five fundamental photons transition, (or with 2 photons of the second harmonic plus one of the fundamental) similar to scheme 1 but the photon energy is increased. Thus the final state of the excitation lies energetically above both the two fine structure levels of the ground state of the Xe^+ ion, namely the $P_{3/2}$ and $P_{1/2}$ ionization thresholds. The subscript indexes represent the total angular momentum of the Xe^+ ion that is left behind after the ionization. The   energy difference of the two thresholds is $10537 cm^{-1}$. An intermediate resonance reached in this case is the bound $4f[3/2]_2$ state and the fundamental wavelength used is about 440nm. The decay of the final state to the two continua results in emission of photoelectrons with different Kinetic energies.

$$E_{Kin} = n\hbar\omega_1 - E_{thr} = m\hbar\omega_2 - E_{thr} \qquad (2.4)$$

Where $\hbar\omega_1$ and $\hbar\omega_2$ are the photon energies of the fundamental and the harmonic field and n,m are lowest number of photons in the two channels nexessary for the ionization process. E_{kin} corresponds to the kinetic energy of the photoelectrons and E_{thr} is the ionization threshold energy.

.

The excitation probability is given by the same formula (2.1) as in scheme 1 but with the effective n-photon electric dipole moment $\mu^{(n)}$ calculated for states of this specific scheme.
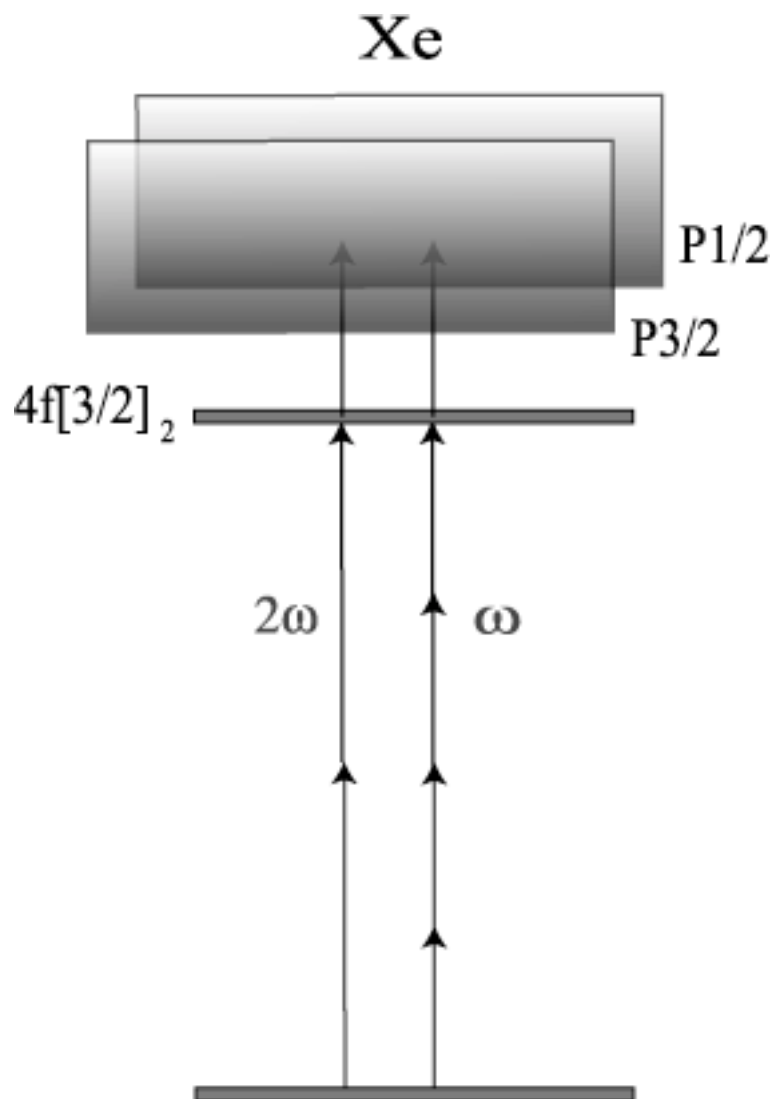
Fig. 2.3 Excitation above both Xe thresholds.

3. Experimental Set up

3.1 Laser Source

.

3.1.1 Dye laser

Organic dyes have a large range of wavelengths over which amplification can occur (gain bandwidth). Therefore laser sources with gain medium as organic dyes can deliver coherent light spanning a large range of colours in the spectrum. This is the principle of operation in a dye laser. The wavelength of the laser light is selected through the adjustment of a prism or grating. An outline of a tunable dye laser is shown in Figure (3.2). Since the dyes used in tunable dye lasers are fluorescent, another light source is used to 'pump' the dye and cause the population inversion. The pump beam used to excite the large dye molecules and produce the population inversion is in the present case an excimer XeCl laser which delivers laser pulses of 20ns duration and about 300mJ energy per pulse at 308nm wavelength. Some input energy will be absorbed in the form of vibrations or heat, for that reason the dye solution is pumped out of the optical cavity by a circulator in order to prevent any part of the dye from becoming exhausted during the excitation process. In the present experiment the dye Rhodamine 6G has been used, the emission spectrum of which ranges between 500nm and 630nm. The energy absorbed by the dye creates a population inversion, moving the electrons into an excited state. The dye molecule decay

.

spontaneously into a relatively long-lived 'metastable state', where it awaits stimulated emission. The optical configuration of the dye laser used is depicted in figure (3.2). We identify two stages, the oscillator-preamplifier and the amplifier stage. In the first part one recognizes the front cavity mirror down to the right, while the back mirror is a reflection gratting in Littow configuration reflecting back into the cavity only the desired wavelength. The gratting is mounted on a adjustable angle deck which is controlled by a stepper motor. The dye solution is located in a transparent cuvete which is illuminated with the pump beam. A small portion of the resonator beam is coupled out of the cavity by a reflection from the prism shown in the diagram. The small signal pulses passes one more time through the cuvete (although at a different height) and gets preamplified. The output of the preamplifier is coupled into a telescope where the beam diameter and position is adjusted. Finally the beam gets amplified in the amplifier cuvete on which most of the pumping intensity is put in. Since the dyes commonly employed are large and have many lower-energy states available for the excited electron to decay into, a large range of output wavelengths is available to the dye. The dyes most commonly and successfully used in dye lasers are dissolved in a liquid. In spite of the large gain bandwidth of organic dyes, one dye cannot cover the entire visible spectrum. So in order to scan a large wavelength range one has to change several dye solution or use a mixture, although the later is not recommended. The resulting duration of the output pulse is the same as the duration of the pump i.e. 20nsec.

.

Excitation (pump pulse)

Upper Excited states

Photon

Lower Excited states
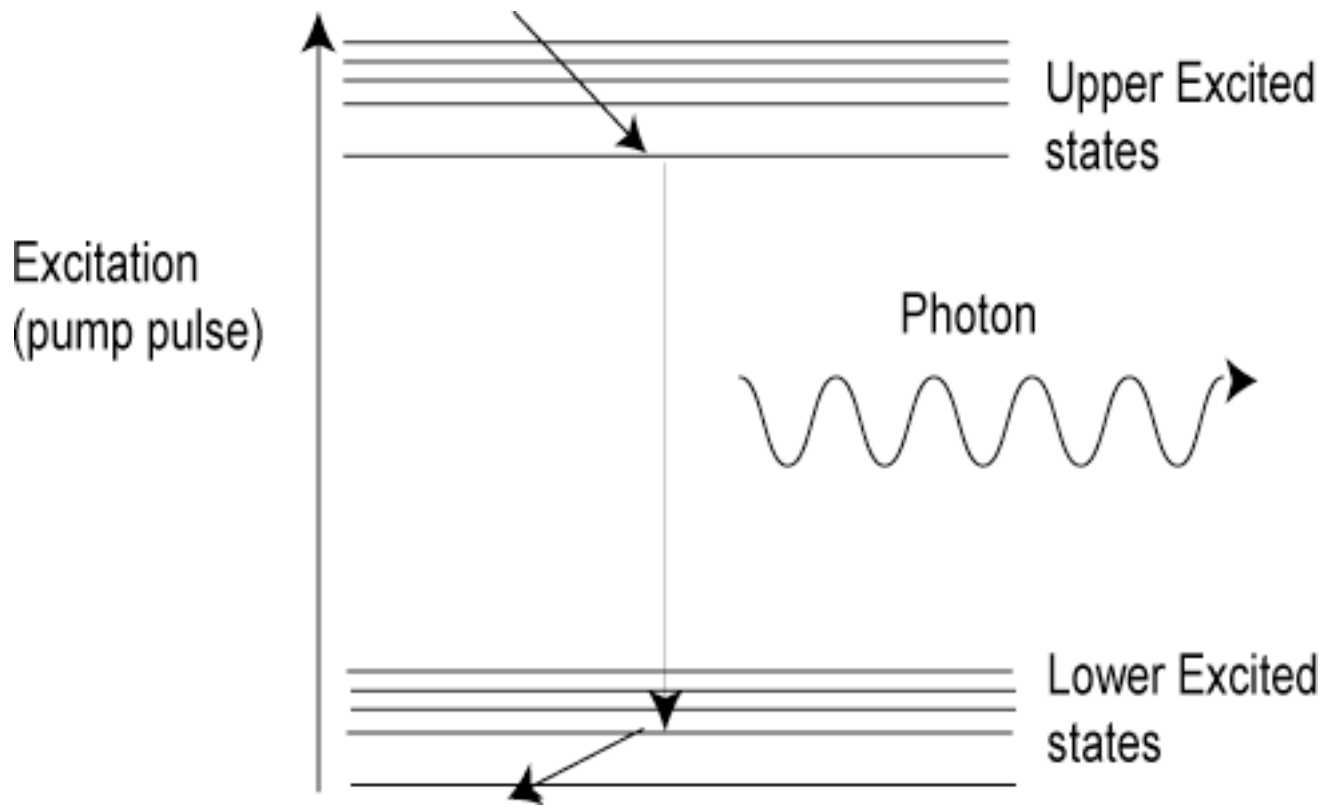
Fig.3.1 Dye laser excitation scheme.

.

Fig. 3.2 Dye laser optical configuration

3.1.2   MOPO all solid state laser

The operation principle of an optical parametric oscillator is to convert the one fundamental wavelength, which is delivered from a frequency doubled Nd:YAG laser, into a continuously tunable wavelength. This is achieved through an non linear parametric process where one high frequency photon is annihilated and two lower frequency photons are created, i.e.:

$$\omega_{pump} = \omega_{signal} + \omega_{idler} \tag{3.1}$$

The later equation states that the photon energy is conserved. In addition, photon momentum is conserved as well, which translates into:

$$k_p = k_s + k_i \tag{3.2}$$

where (p)ump, (s)ignal, and (i)dler are the traditional assignments given to the input photon, and generated photons of higher and lower energy, respectively. The specific pair of frequencies that is produced is determined by this momentum-, or phase-matching condition.

.

The specific laser used in our experiments is a commercial Spectra-Physic MOPO-SL system and can tune continuously from 410nm to wavelengths grater than 4000nm delivering pulses of 3-4 nsec duration. The non linear medium used is a BBO crystal mounted on adjustable angle mount so that one can tilt the crystal axis to meet the phase matching condition (i.e. equation 3.2).

A simplified layout of the optical configuration is depicted in figure (3.3). It consists of two major parts, the parametric oscillator (OPO) and the parametric amplifier (OPA). In both cases the nonlinear medium is a BBO crystal pumped by the doubled Nd-Yag laser beam which is guided with 355nm dichroic mirror. The pump beam size is adjusted with telescopes and finally gets dumped on beam blockers. The pumping of the OPA is delayed so that it coincides temporarily with the signal beam from the oscillator. The OPO cavity consists of a high reflection broadband mirror and a reflection gratting which is used to select a narrow bandwidth output. The signal beam is then seeded into the OPA cavity which consists of a high reflection back mirror and a partially reflective output coupler. The output beam is also frequency filtered by multiple reflection on special IR dicroics to be separated from the idler beam. The later filtering is not depicted in figure (3.3).

.
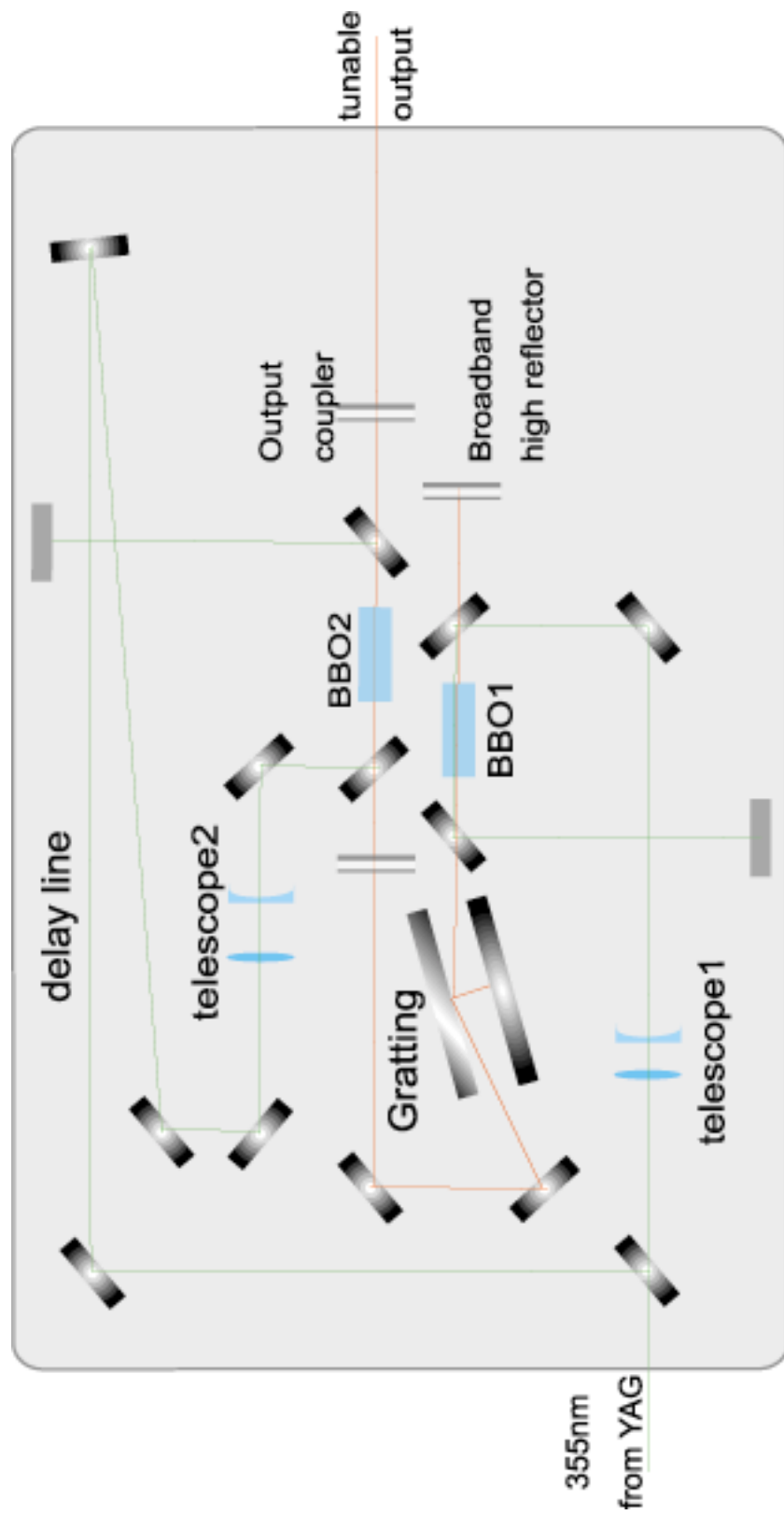
Fig 3.3 Mopo optical configuration

3.2   Phase – Amplitude Adjustment

.

3.2.1   On axis configuration

The laser beam from the laser source is doubled in a type I BBO crystal. The polarization of the field produced is perpendicular to the polarization of the fundamental field. The conversion efficiency of such a crystal is about 30%. The output of the crystal is a two color field of frequencies ω_1, ω_2 where $\omega_2 = 2\omega_1$ that propagate collinearly with perpendicular polarizations. The two beams are coupled into a Soleil-Babinet compensator, the orientation of which is chosen so that its two optical axes are parallel to the two polarization planes of the two fields (fig. 3.5) . In this arrangement the Soleil-Babinet compensator is used as a variable-thickness optical plate and not as polarization retarder as is usually the case. Utilizing the normal dispersion characteristics of the quartz material from which the compensator is made, the relative phase between the two wavelengths can be controlled in a reproducible way. The dispersion characteristic of the crystal quartz can be calculated by the following polinomial:

$$n_i = B_1 + B_2\lambda^2 + B_3\lambda^{-2} + C_1\lambda^{-4} + C_2\lambda^{-6} + C_3\lambda^{-8} \qquad (3.3)$$

.

Where λ is the field wavelength in μm and i stands for ordinary and extraordinary axis of the crystal. The constants B_j, C_j j=1,3 are listed in table (3.1).

The soleil-babinet retarder consists of a movable part which is a crystal wedge. The horizontal position of the wedge is adjusted by a micrometric driver. The wedge angle was measured with a He-Ne laser by monitoring the distance between the reflections from the front and back surface as depicted in figure (3.6). The angle was found 3E-3rad, therefore a 2π rad change in the two color fields relative phase can be achieved by translating the crystal wedge a distance of few millimetres. The exact period distance depends on the exact wavelength and is calculated for each case.

A linear polarizer, placed behind the Soleil-Babinet retarder, is employed in order to select the appropriate field amplitudes in a common polarization plane, the polarization plane of the polarizer. The two excitation quantum amplitudes can, in this way, be easily adjusted by rotating the polarizer so as to transmit the required field-amplitude component of the two beams.

.

Constant	**Ordinary axis**	**Extra-ordinary axis**
B_1	2.3849	2.35728
B_2	-1.26E-02	-1.17E-02
B_3	1.08E-02	1.05E-02
C_1	1.65E-04	1.34E-04
C_2	-1.95E-06	-4.45E-07
C_3	9.36E-08	5.92E-08

Table 3.1. Crystal quartz dispersion constants.

.
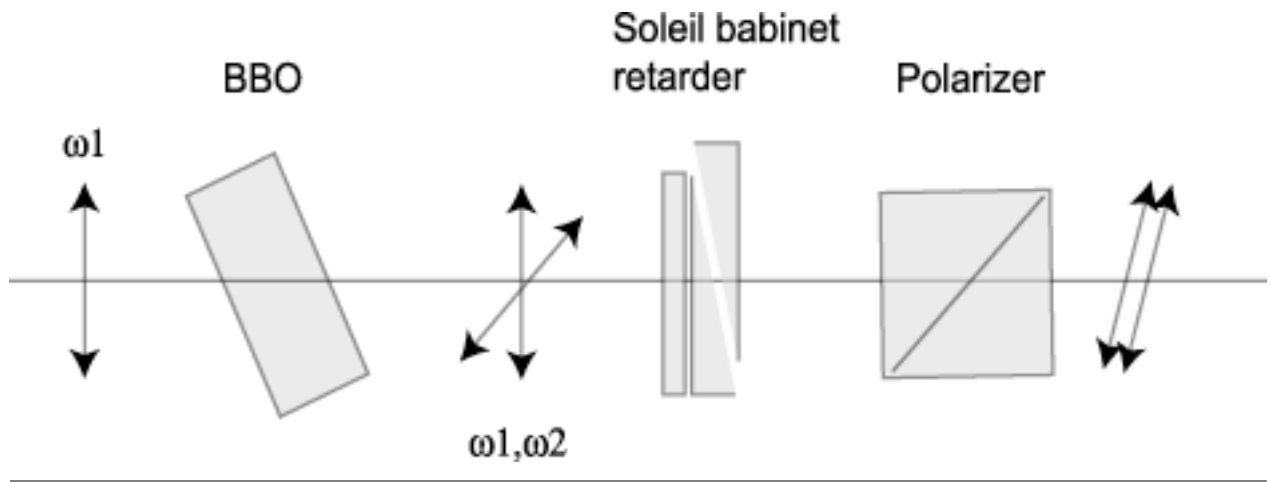
Fig. 3.4 Experimantal setup for phase-amplitude adjustment
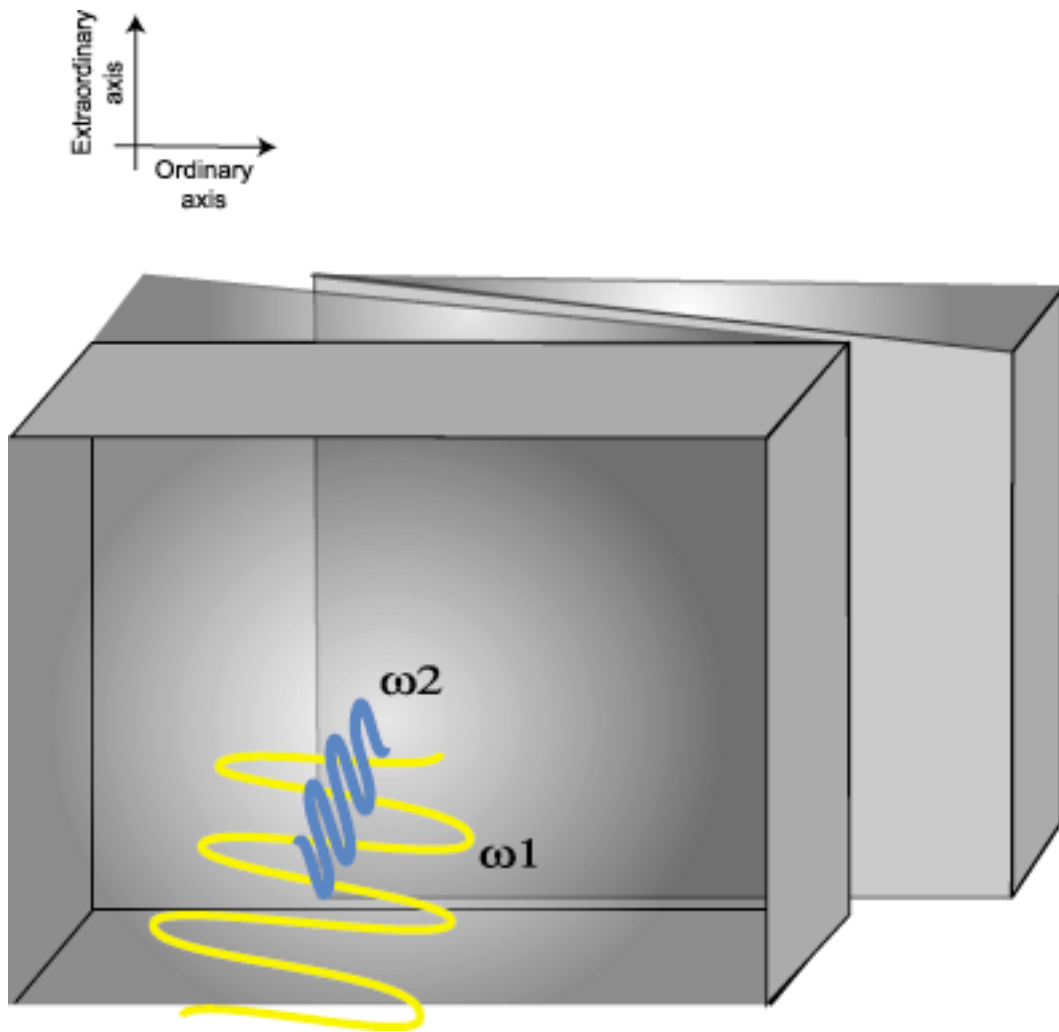
Fig.3.5 Phase adjustment using movable birefrigent (soleil babinet) wedge.

.
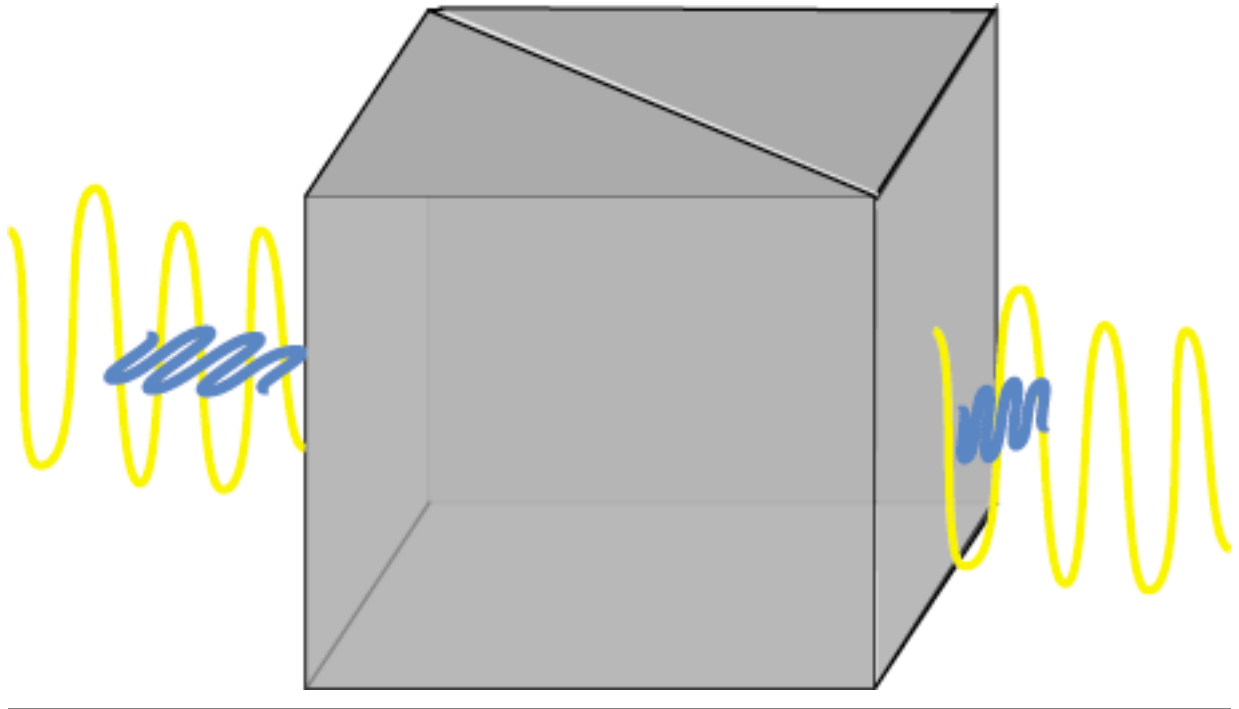
Fig3.6. Amplitude adjustment with polarizer
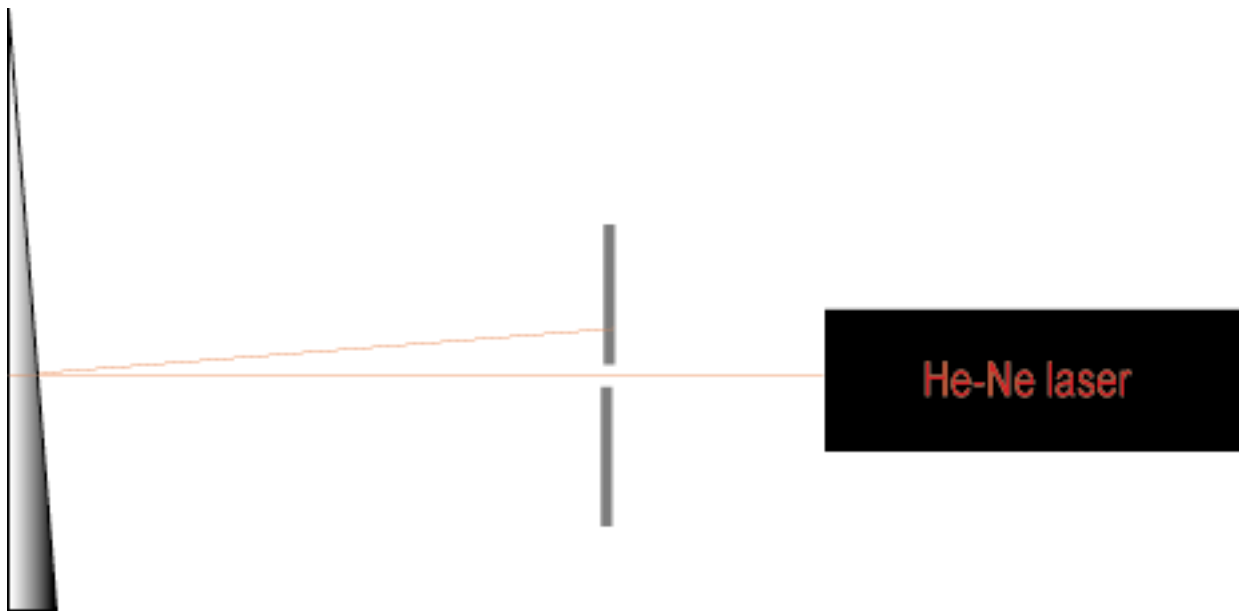
Fig 3.7. Measurement of the crystal wedge angle

.

3.2.2   Mach Zender configuration

An different method for phase and amplitude adjustment is tested, in which
unlike in the previous on axis configuration differs, the two different frequency
beams are propagating in different axis in a configuration similar to the Mach
Zender interferometer as depicted in figure (3.8). Initially a portion of the laser
beam (~5%) is reflected on a quartz plate and directed into the SHG crystal. The
two colours propagate on different axis and recombine at a dicroich at the output
of the interferometer. Extra care is taken that the optical path, taking into
consideration normal dispersion in the several optics, is approximately equal for
both fields in order to achieve maximum temporal overlap of the laser pulses.

The relative phase adjustment is accomplished by slowly varying the optical
path of the second harmonic branch by coupling it into the soleil babinet with
the polarization axis coinciding with the extra ordinary propagation axis. The
fact that the fundamental ω field is not propagating through the soleil babinet
reserves a lot of fundamental intensity since the later element consists of 6
interfaces not to mention the scattering from defects on the surfaces.

The amplitude adjustment is accompliced by interfering a variable attenuator in
the reflection heading to the SHG crystal. Finally the polarization of the
harmonic field is tilted by 90degrees in order to interfere with the fundamental

.

filed. The later is accomplished using a double Fresnel rhomb tilted at 45degrees from it's vertical position.

From the previous it is apparent that this configuration advances, in comparison to the on axis one, on the fact that the fundamental field propagates through minimum number of optical elements, therefore the ω field intensity is reserved, a very important factor in experiments where no intermediate resonances are involved, like in the control scheme of the AIS of Mg.

.
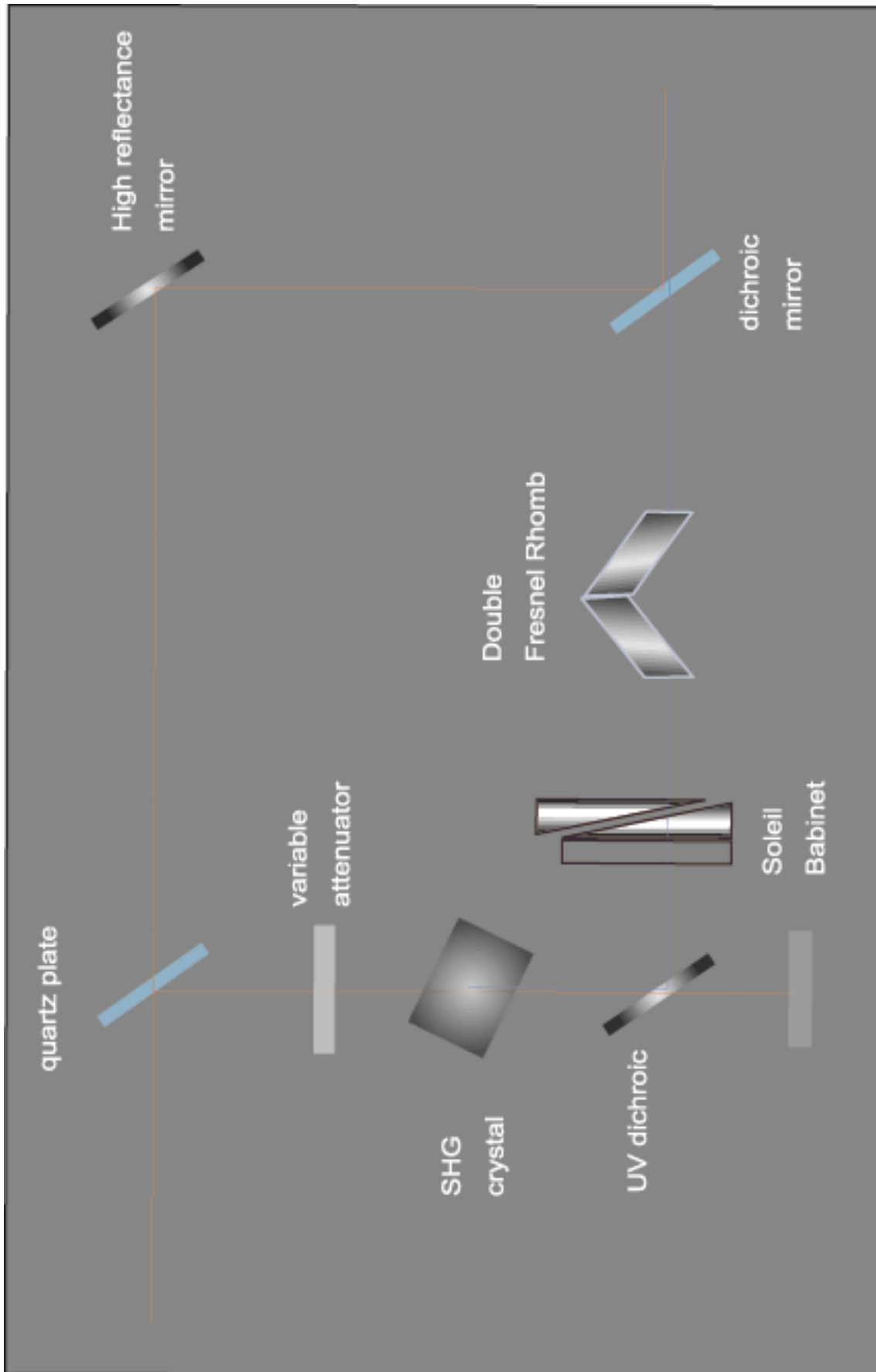
Fig3.8 Mach Zender configuration

3.2.3   Phase measurement

In this chapter we introduce a method of measuring the relative phase the two coulor coherent laser fields. In the concept of the classic interferometric techniques the relative phase of two coherent fields can be measured provided that they have the same or close frequencies. When the fundamental field and its second harmonic field are involved these techniques cannot be applied, instead one can use a non linear process, like harmonic generation. Specifically in the on axis configuration one can sample the two colour beam taking a weak reflection of the phase adjusted fields that come out the soleil babinet using a quartz plate and couple the reflected field into a second SHG crystal. When the later is on phase matching condition the extra harmonic field produced will interfere with the initial part resulting in constructive or destructive interference. For reasons explained in Appendix C the extra harmonic field carries the information of the phase of the fundamental field. Therefore one can acquire the measure the relative phase between the initial two colour fields by measuring the intensity of the harmonic field after the second SHG crystal. The experimental setup is depicted in figure (3.9), where one recognizes a UGL5 filter used to

.

filter out the fundamental field. The transmittance for the later field was checked so that the no fundamental signal was measured after the filtering.

The above approach of the interference is only qualitative in order to give an insight of the processes involved. In order to acquire quantitative results for the relative phase one has to solve the Maxwell equations (see Appendix C) for the propagation of the two fields into the second BBO with the appropriate boundary conditions taking into account also the dispersion of the fields the optics that the two fields propagate through. The discussion of the precise measurement of the relative phase is continued in a later on chapter.
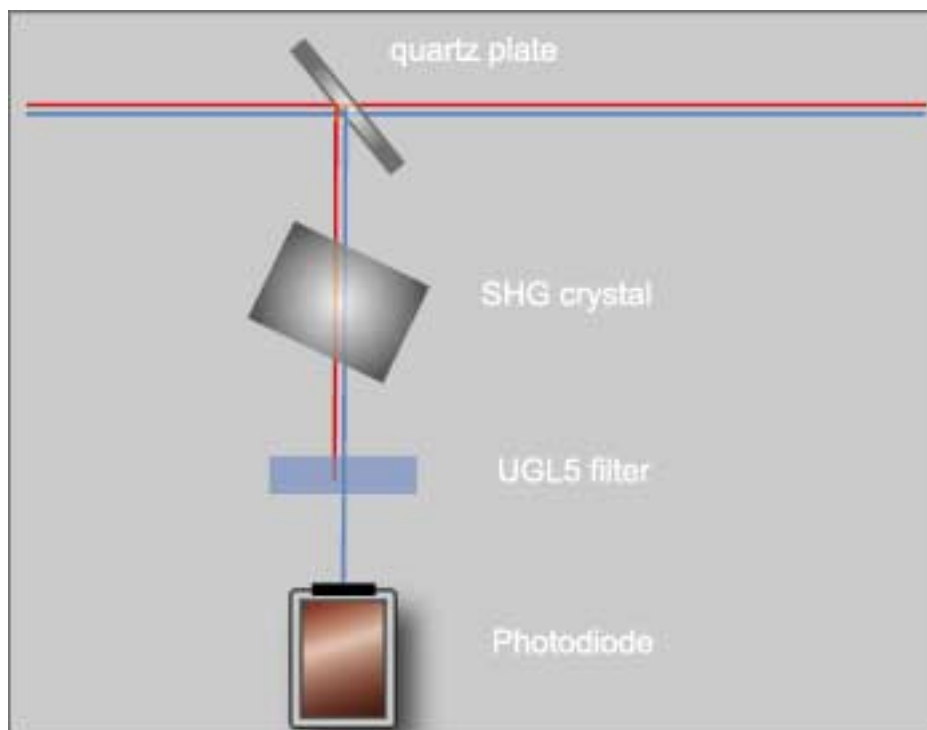
Fig3.9 Optical configuration of the phase measurement setup.

.

3. 3 Detection systems

3.1.1   Gas cell

In order to measure the ionisation yield both beams are focused by means of an achromatic lens of 12-cm focal length into an metal chamber, namely the ionization cell. The cell is equipped with two quartz windows which are sealed with rubber o-rings. The cell is filled with a few mbar of Xe gas and equipped with a charge collector. The collector is biased with high voltage forcing the produced ions to meet the metal surface of the charge collector. A current flow is created in this way which is measured with a digital 400MHz Lecroy oscilloscope monitoring the voltage drop on a 50Ω resistor. Also a 500pF capacitor is introduced which cuts the DC component of the voltage and allows only the AC signal to go through to the oscilloscope.   This detection system is depicted in figure (3.9).

.
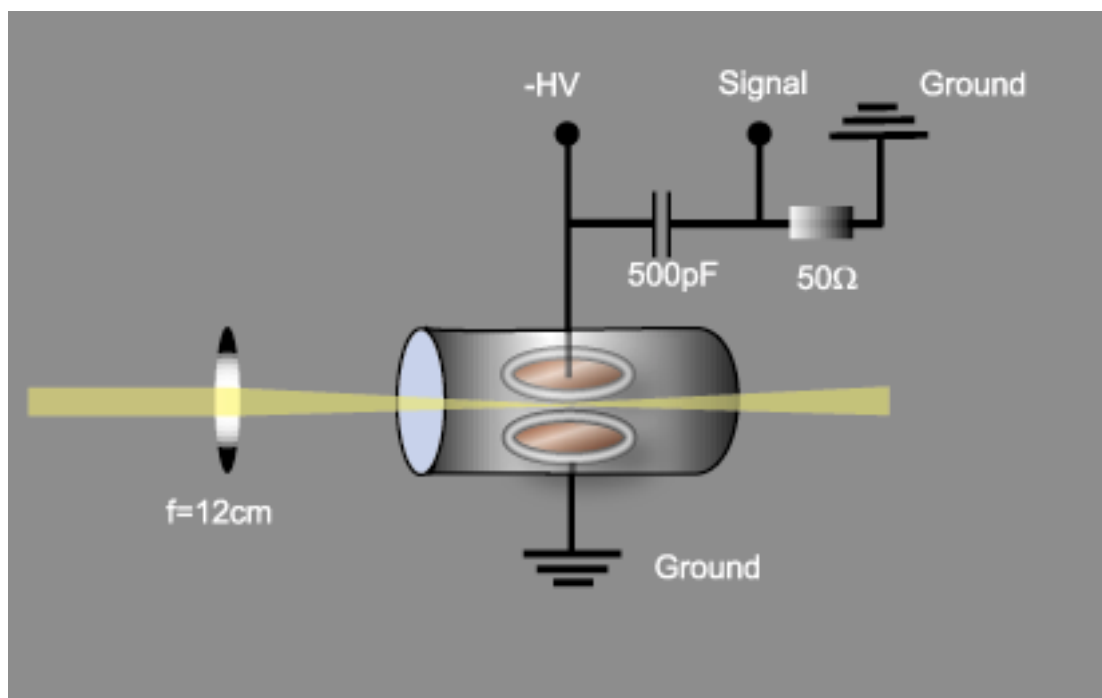
Fig3.9 Ionization cell configuration

3.3.2   Ion time of flight spectrometer

Separation of different ions is accomplished using time of flight (TOF) mass spectrometry. The basic idea is based on the fact that for a fixed kinetic energy E the mass m and the velocity u of the ions are correlated therefore ions of different masses acquire different velocities when accelerated to the same amount of kinetic energy:

$$m = 2E / u^2 \qquad (3.4)$$

By measuring the time T the ions need for travelling a fixed distance s the velocity u and from the above relation the mass of the ions can be calculated. Typically the length of the flight path in TOF spectrometer systems is about 0,1 - 1m. Similarly to the ionisation cell an extraction field is used in the interaction region accelerating the ions to energies up to 2 KeV. For these conditions the flight times are 5 to 100 μs, while the width of individual TOF peaks is a few ns. Of course all the ions start the travel through the spectrometer at about the same time since the interaction with the laser pulse lasts only an interval of a few nsec. To insure that the ions are not destructed by any external electric field the flight path is surrounded with a metallic tube equipped with metal grids on both

47

.

ends. The ions are finally detected employing an multichannel plate (MCP) detector. The detector used is a Hamamatsu double microchannel plate in a chevron configuration delivering a gain factor of 10^7, response time less than 1 ns and a high sensitivity (single ion signal > 2 mV without further amplification). A basic requirement for the operation of the detector is vacuum conditions better than 3×10^{-5} mbar, therefore the TOF apparatus is pumped by a ALCATEL turbomolecular pump which is backed by a rotary mechanical pump from the same company. The atoms are brought in the interaction region using effusive beam techniques. In order to create an effusive beam of Xe atoms a pulsed electromagnetic nozzle was used. By applying a synchronized to the laser trigger signal on the nozzle driver the Xe atoms are brought to the interaction region right when the laser pulse arrives. In the case of Mg atoms one cannot use this technique since the Mg sample has to be heated up to 600 ^{o}C in order to produce metal vapour. For this reason an oven was inserted at the top of the interaction chamber filled with magnesium pellets which, when heated, produced an atomic beam. In both cases the atomic beam met the laser beam and the time-of-flight tube at right angles.

.
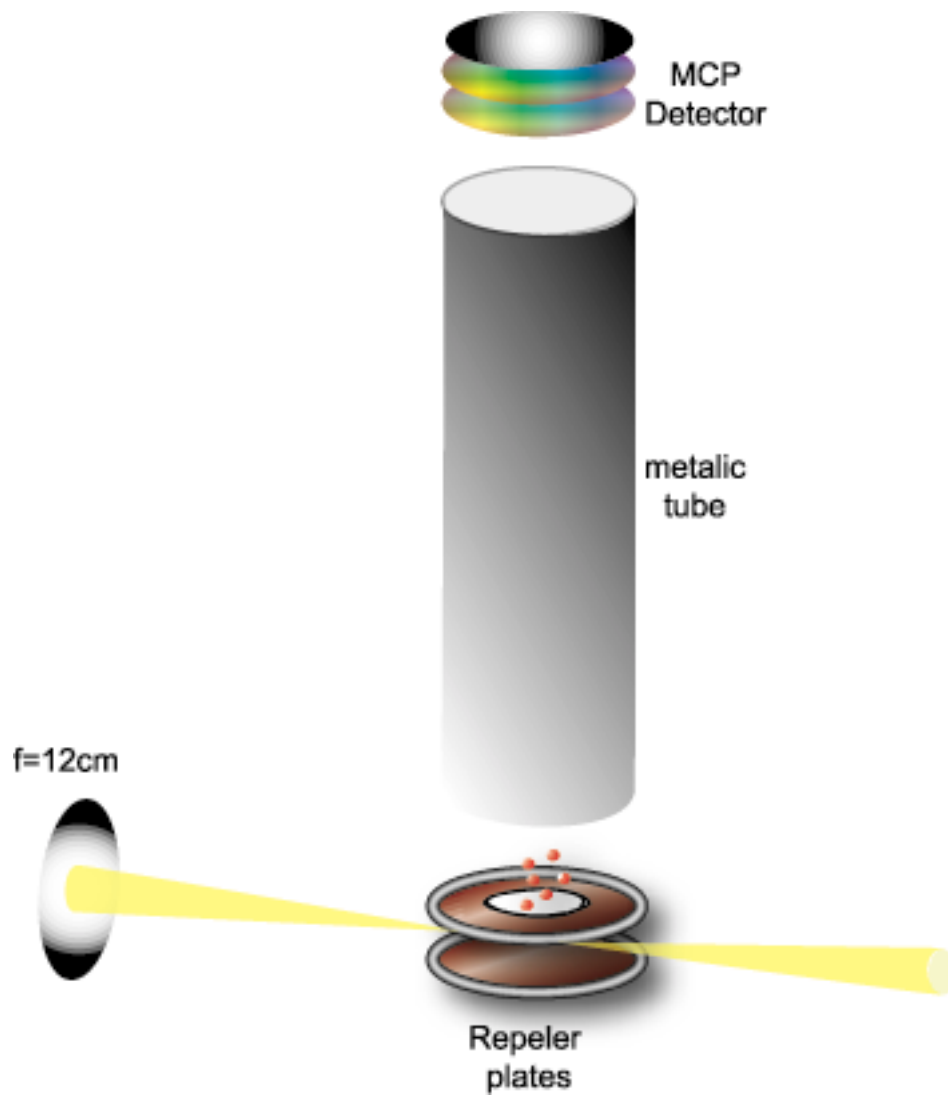
Fig3.10 Time of flight spectrometer.

.

3.3.3 Photoelectron time of flight spectrometer

With the ion TOF technique the total ionization yield is measured. In order to get a better insight into the excitation process one has to measure the kinetic energy of the photoelectrons produced during the ionisation process which is given by:

$$E_{kin} = n \times \hbar\omega - E_{th}$$
(3.5)

Where n is the number of photons absorbed, $\hbar\omega$ is the photon energy, and E_{th} is the ionisation threshold for the given element.

To measure the kinetic energy of photoelectrons a time of flight technique is addressed. For that reason the ion TOF described before is modified, that is the photo electrons are not accelerated by any extraction field, but travel with the kinetic energy defined by the later equation. Because of their small mass, the photoelectrons get easily distorted during their time of flight by both static electric and magnetic fields. For this reason the M-metal tubing that sealed the flight path was used which has the property of blocking the magnetic field because of its large magnetic susceptibility. The last modification regards the applied high voltages on the MCP detector. The different voltage configurations for ion and electron detection of the MCP are listed in the table below.

.
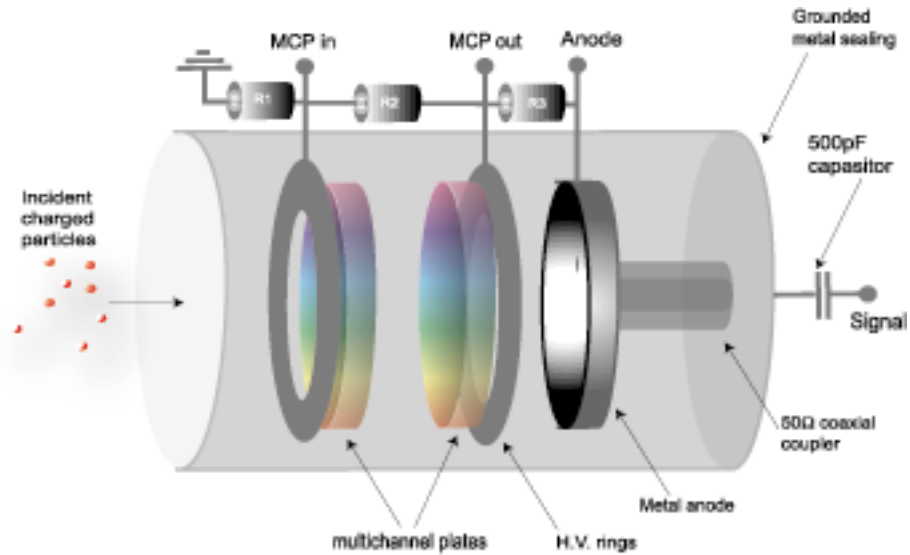
Fig. 3.11 Electrical configuration of the multi channel plate detector

Connection	Applied voltage for ion detection (Volts)	**Applied voltage for electron detection (Volts)**
MCP in	-2000	+300
MCP out	grounded	+2000
Anode	+100	+2800

Table 3.2 Detector bias for ion and electron detection

.

4. Conducted Experiments

.

4.1   Control of the ionisation ratio

The aim the first experiment is to demonstrate control on the transition ratio of the excitation from the ground state to the 6p[3/2]$_2$ bound state of Xe by varying the relative phase of the fundamental and second harmonic field as described previously in scheme one. The laser beam is delivered by the excimer-pumped dye laser. The wavelength of the fundamental is tuned to 504.97 nm, this brings the four photon and two photon transitions exactly resonant with the bound state mentioned before, while the fundamental field energy is 2.8mJ per pulse. For this energy the fundamental field intensity in the interaction region is 10^9 W/cm^2. The phase and amplitude adjustment of the fields is verified via the on axis configuration and the intensity of the second harmonic field is such that the quantum amplitudes of the two photon and four photon transitions are almost equal. The later is accomplished by measuring the ion yield from each channel separately and reducing the second harmonic down to 0.3mJ per pulse where the two signals are made equal. Both beams are focused by means of an achromatic lens of 12-cm focal length into the ionization cell, which is filled with a few mbar of Xe.

.

In order to avoid artefacts from possible polarization rotation, the ion yield of each channel is measured separately as the soleil babinet retarder wedge is displaced. That is to find that the signals exhibit no periodical modulation.

It should be mentioned that for these intensities the one photon transition from the 6p[3/2]$_2$ state to the continuum is saturated. Therefore the ion yield measured monitors the population which is transferred to the 6p[3/2]$_2$ state.

By tuning the relative phase of the two fields through the Soleil-Babinet adjustment, the phase difference $\Delta\theta$ is varied. A strong modulation of the ionization signal could be observed as a function of the Soleil-Babinet wedge position as shown Fig. (4.1). The solid line is a least square fit of the function:

$$y = (1 + Ax) \times \left[B + C \sin\left(\frac{x}{D} + E \right) \right]$$

(4.1)

The modulation depth, defined as $I_{max} - I_{min} / 1/2(I_{max} + I_{min})$, where I_{max} is the maximum and I_{min} the minimum ion signal of the modulation, has a maximum value better than 0.8 in the present experiment and is close to the highest values obtained in phase-control experiments. The modulation depth can be adjusted through (i) the spatial overlapping of the two beams, which can be optimized by carefully adjusting the phase matching of the BBO crystal to minimize beam walk off, and (ii) the angle of the polarizer, an adjustment that controls the relative amplitudes of the interfering excitation channels.

.
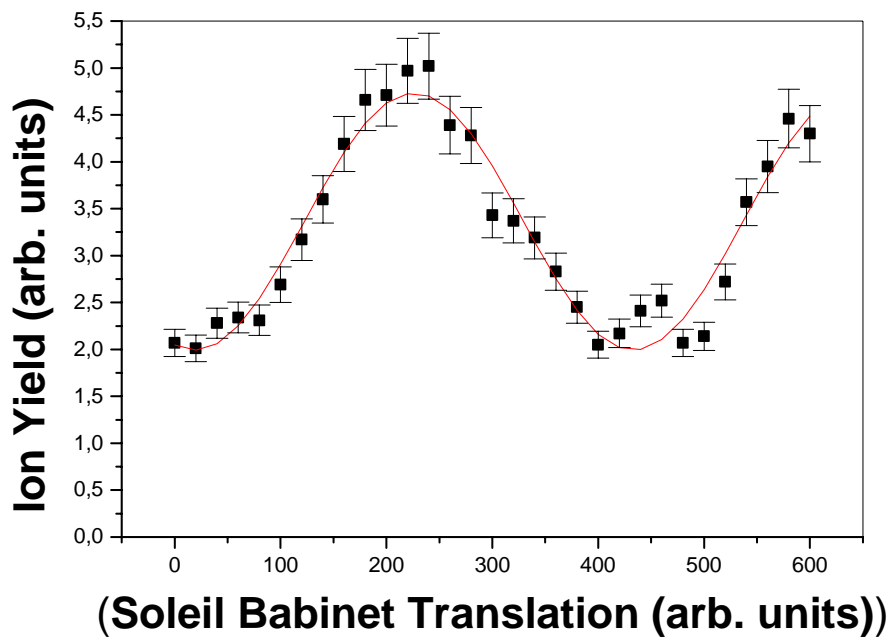
(a)
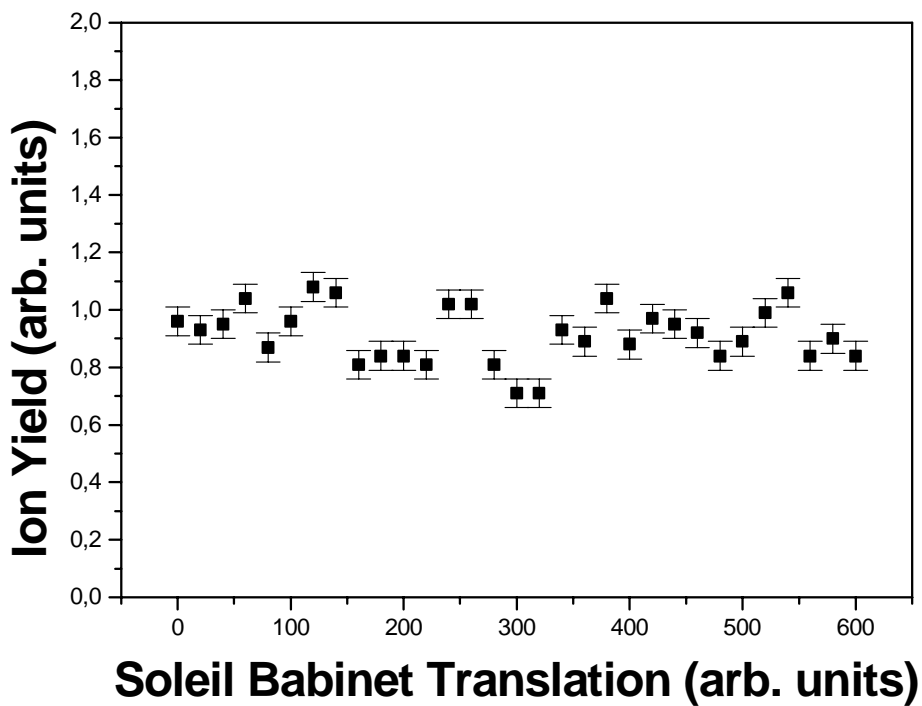
(b)
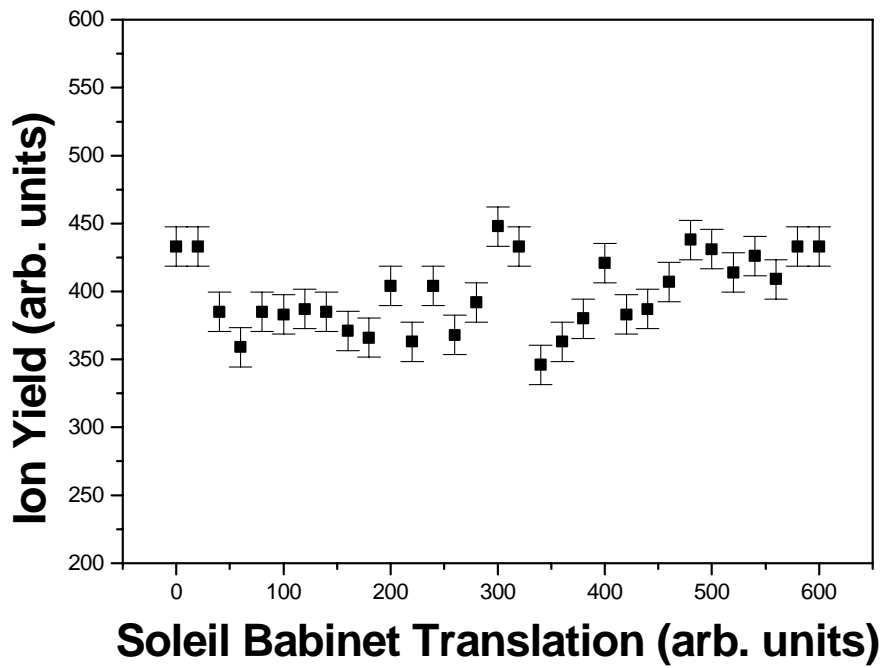
(c)

Fig.4.1 a) Modulation of the ionization yield as function of the relative phase in the presence of both fundamental and second harmonic field, b) and c) control measurement of the ionization in the presence of fundamental only and second harmonic filed only respectively.

.

4.2   Control of the Autoionization

In the second experiment it is our intention to demonstrate control of the excitation to an AIS and the AIS profile utilizing the 4+2 scheme. For this reason scheme 2, as described before, is employed. In order to determine the appropriate experimental parameters, previous work done in our group as well as theoretical calculations were proved helpful indeed. In figure (4.2) the two photon profile of the $3p^2$ AIS is depicted, measured by Y.L. Shao et.al [27].

In figure (4.3) and (4.4) the calculated cross sections in the vicinity for the $3p^2$ AIS for the two photon and the four photon transitions are depicted [28]. The sharp features observed origin from intermediate bound state resonances within the multi photon excitation while the small increase of the crossection indicated on the graphs origins from the AIS state.

With these values the saturation intensity for the four photon transition   is calculated 10^{12} W/cm^2 order of magnitude. For details on the calculation the reader is referred to appendix D.

.
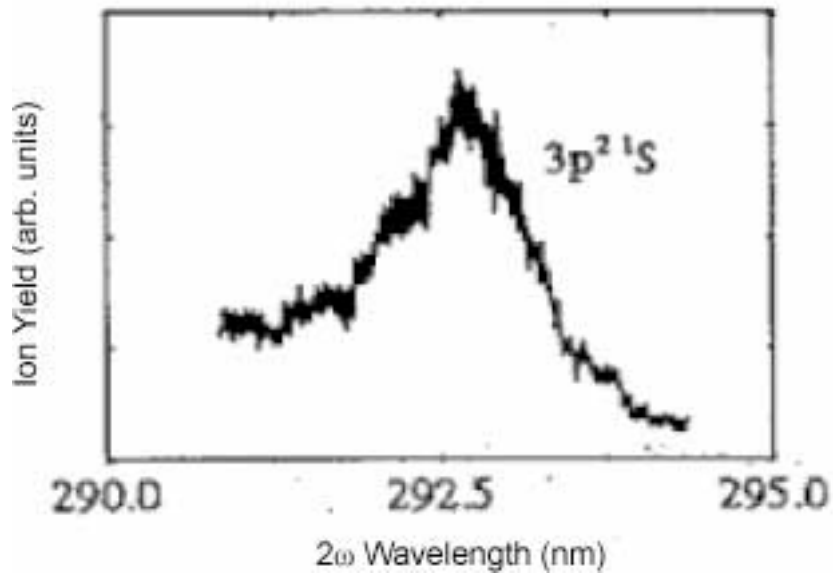
Fig.4.2 Two photon AIS $3p^2$ resonance [27]
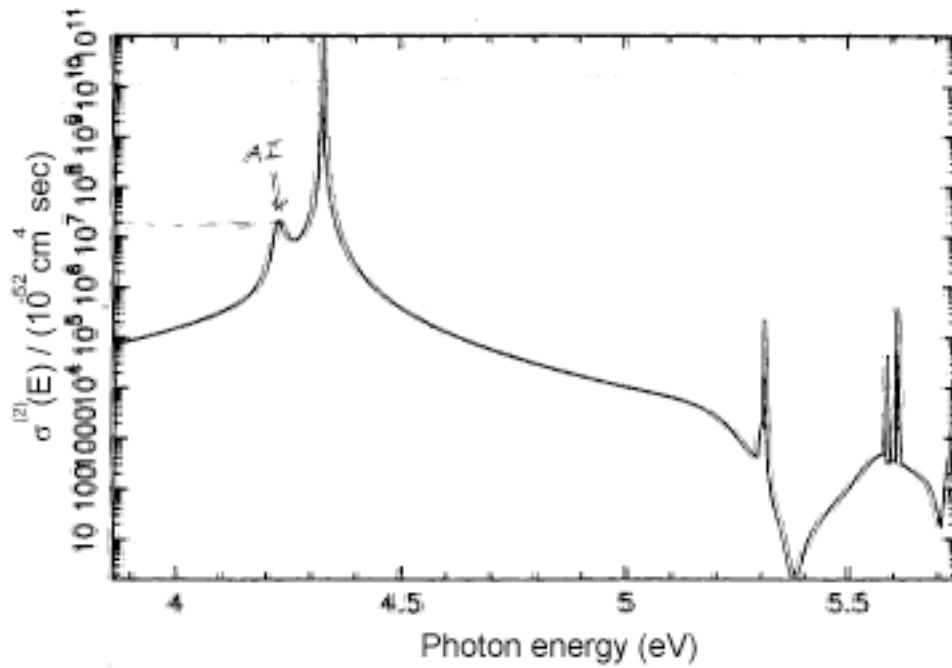
Fig4.3. Calculated cross section [28] for the two photon transition in the vicinity of $3p^2$ AIS state of Mg

.
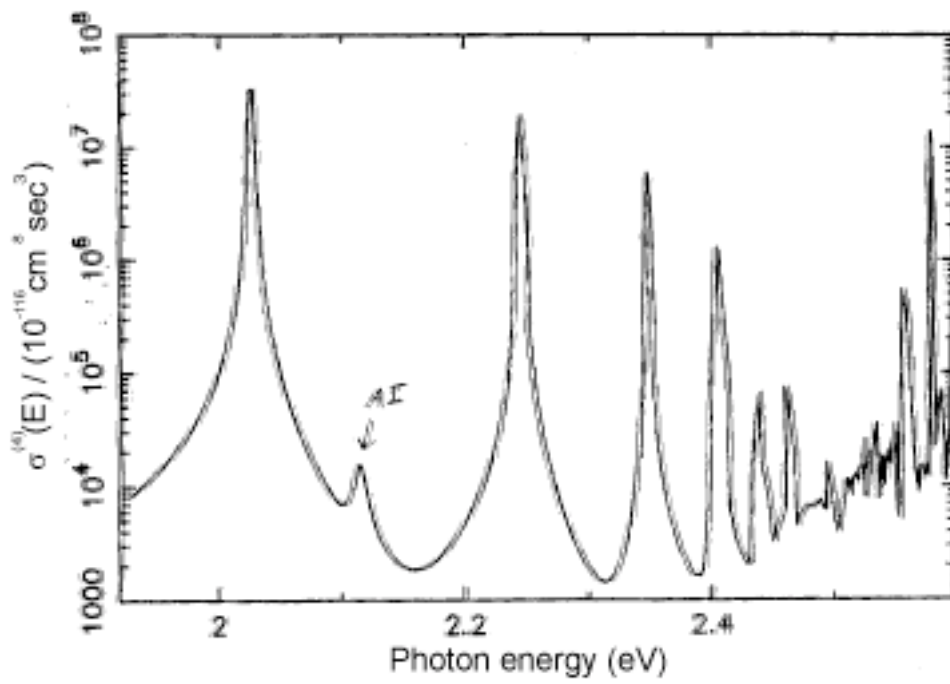
Fig4.4. Calculated cross section [28] for the four photon transition in the vicinity of $3p^2$ AIS state of Mg

The density of Mg atoms in the interaction region that is delivered by an oven as an effusive beam is about 10^{11}cm^{-3} (estimation based on the setup geometry [38]). In order to have the desired signal to noise ratio for the four photon transition, the required intensity of the fundamental field is estimated to be 10^{11}W/cm^2. Such intensities cannot be delivered by the available Dye laser system, nevertheless the all solid state MOPO system with an output energy of 80mJ per pulse is proved a perfect solution for this problem. The measured profile of the 3p^2 AIS for the four photon transition is depicted in figure (4.5). The AIS profile is measured for several intensities. The linear fit of the intensity dependence graph exhibits a slope of 3,5 which is in close agreement with the expected value.

From the calculated cross sections we extract that equal quantum amplitudes for the interfering channels are obtained when the second harmonic field intensity is 10^8W/cm^2 , therefore for these intensities maximum interference is expected.

Experimentally equal amplitudes are obtained by equalizing the signal from each channel separately referring to the centre of the AIS resonance at λ_ω=585nm.

.
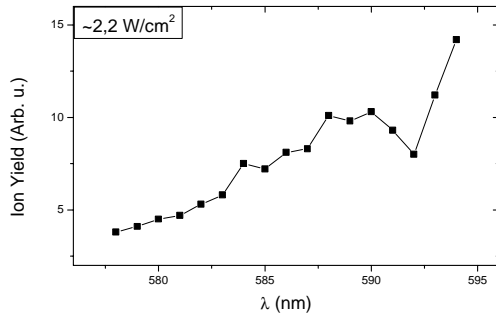
(a)
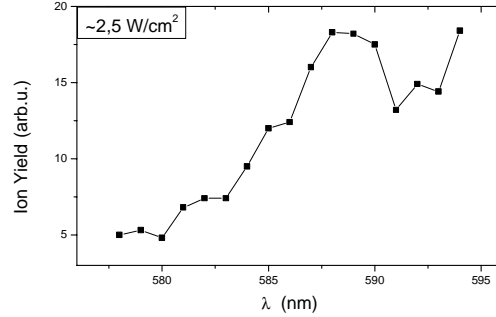
(b)
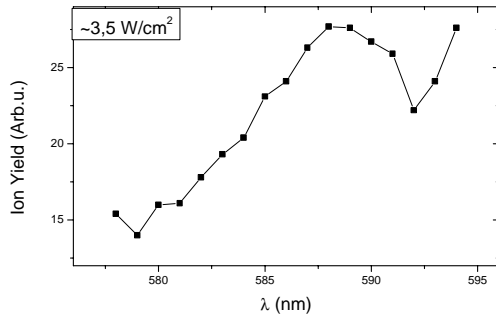
(c)
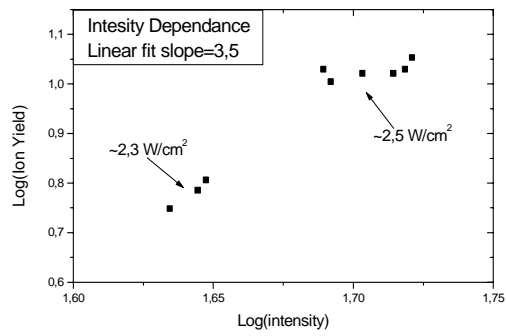
(d)

Fig 4.5. a),b),c) Measurement of the $3p^2$ autoionize Mg state profile using 4-photon excitation scheme for various intensities of the excitation field. d) Intensity dependence diagram of the ionization signal exhibiting a 4th order nonlinearity and also indicating the saturation intensity for the 4-photon excitation.

.

This measurement of the dependence of the autoionization profile on the relative phase of the fields cannot be made in a straight forward manner because scanning the wavelength of the two fields involves rotation of optical elements like the SHG crystal. The later results in a non fixed value of the relative phase and therefore a different approach should be pursued. One the other hand one can scan the relative phase for different fixed values of the wavelength within the AIS resonance. The suggested plan involves measuring simultaneously the modulation of the ion yield and the relative phase of the laser fields. Combining these measurements one is able to reconstruct the resonance profile for different values of the relative phase. These measurements are presented in figures (4.6) and (4.8). For the simultaneous ion yield plus phase measurement the on-axis optical configuration is used while the detection system is the ion TOF. In figure (4.7) a typical mass spectrum is presented, one recognizes the Mg isotopes being resolved. As mentioned before the major drawback, because of the 4th order nonlinearity of the fundamental channel, is the lack of fundamental field intensity resulting in small SNR and loss of reproducibility. For this reason the Mach Zender like configuration was also tested. For this configuration the requirements of phase measurement set-up described in a previous chapter are not met therefore only the ion yield modulation was measured for different wavelengths without the information of the relative phase. Measurements using this configuration are presented in figure (4.9).

.
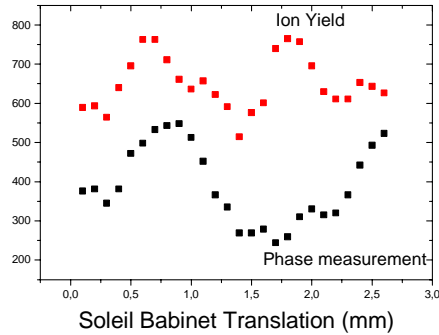
Fig.4.6 Simultaneous measurement of phase control of the ionisation signal in a 4+2 excitation scheme coupled to the $3p^2$ autoinize state of Mg , and the measurement of the relative phase of the excitation fields. The Excitation fields have fixed wavelengths λ_ω=585nm, $\lambda_{2\omega}$=292,5nm. Typical intensity of the fundamental field: 10^{11}Watt/cm^2. Quantum amplitudes of 4-photon and the 2-photon channels measured equal.
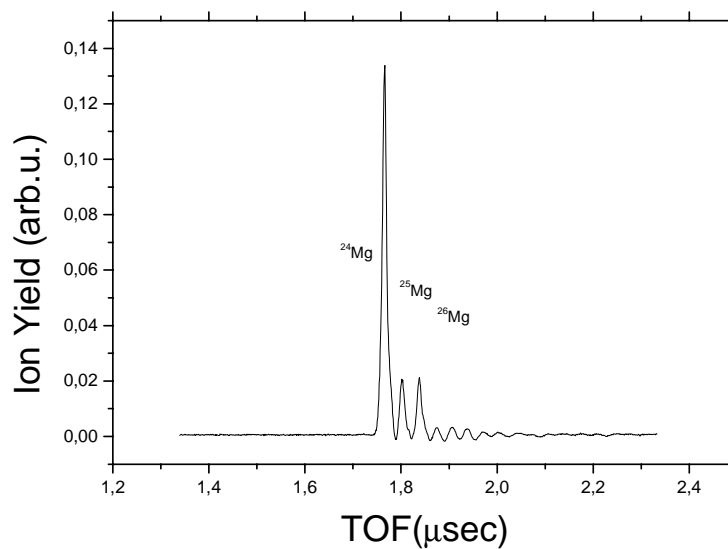
Fig4.7. Time of flight spectrum of ions created by 4-photon excitation at fixed wavelength λ_ω=585nm.

.
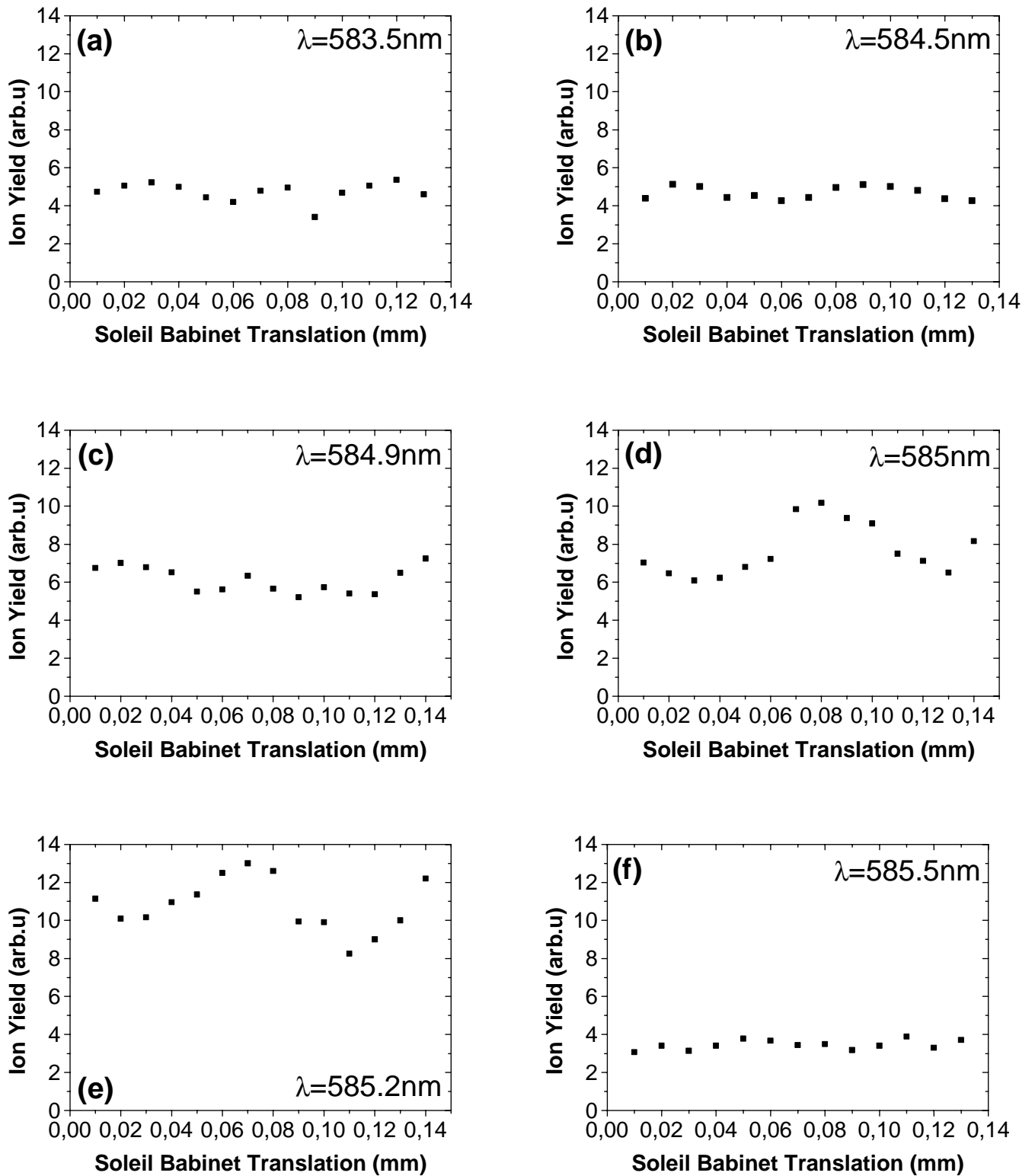
Fig.4.8 Phase control of ionisation Ratio in a 4+2 excitation scheme coupled to the 3p^2 autoionize state of Mg for various wavelengths a)…f). The intensities of the fundamental and second harmonic fields kept constant in all cases. Typical intensity of the fundamental field:

10^{11}Watt/cm^2. The quantum amplitudes of the 4-photon and the 2-photon channels are optimized to be equal at λ_ω=585nm, $\lambda_{2\omega}$=292,5nm.
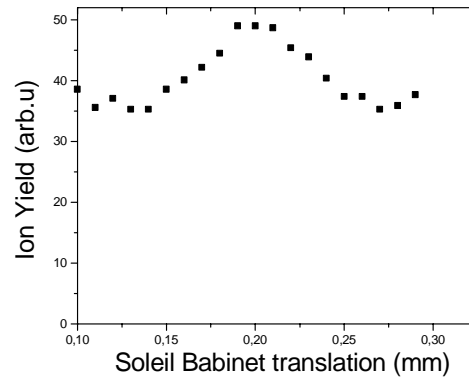
Fig4.9. Phase control of ionisation Ratio in a 4+2 excitation scheme coupled to the 3p^2 autoionize state of Mg for fixed wavelengths λ_ω=585nm, $\lambda_{2\omega}$=292,5nm. Typical intensity of the fundamental field: 10^{11}Watt/cm^2. Quantum amplitudes of 4-photon and the 2-photon channels measured equal.

.

4.3   Control of the branching ratio

In the third experiment we employed scheme 3 involving Xe atoms. In this scheme the final state lies energetically above both ionization thresholds of Xe, namely the $P_{1/2}$ and $P_{3/2}$ thresholds, therefore it is the aim of this experiment to explore the possibility of control over the ratio of the decay into these two continua. In order to acquire a significant signal from five photon channel the fundamental wavelength is chosen such that the excitation scheme is close to resonance with the bound 4f[3/2]$_2$ state of Xe.

In order to determine the threshold in which the final state decays, the photoelectron kinetic energy is resolved using the photoelectron TOF technique. The fundamental field delivered by the excimer pumped Dye laser is coupled into the on axis configuration and both laser field are focused by means of achromatic 12cm lenses.

For several values of the detuning from the 4f[3/2]$_2$ state the modulation of the electron yield from the two continua is measured. The electron yields excibit periodic modulation as function of the relative phase similar to experiment 1,

.

while the two signals modulate in phase independent of the wavelength. Typical graph of the modulation is depicted in figure (4.10). Further comments on the results are postponed for the discussion section.

P$_{3/2}$ threshold ionization

P$_{1/2}$ threshold ionization

Ionization Ratio (P$_{3/2}$/P$_{1/2}$)

Soleil Babinet Translation (arb. units)
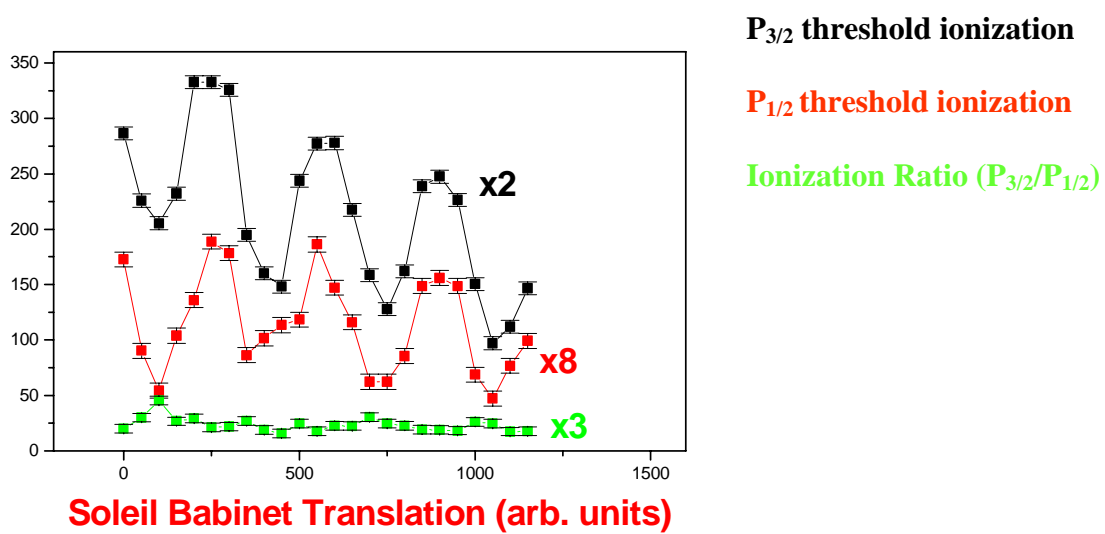
Fig 4.10. Modulation of the ionisation from decay to P$_{1/2}$ and P$_{3/2}$ thresholds of Xe vs relative phase of the laser field.

.

5. Discussion Section

.

5.1 On the experimental setup

Previous work conducted in our lab had demonstrated phase control of ionisation in four-photon resonant five-photon ionization [4+1 resonantly enhanced multi photon ionization, (REMPI)] through the $4f[3/2]_2$ state of Xe, [32], where the second excitation channel of the resonant state included one third harmonic and one laser photon. This excitation scheme is depicted in figure (5.1). One notices, however, that the two-photon excitation channel of the bound state does not need to involve one third harmonic photon and one fundamental photon but can also be reached by absorbing two second harmonic photons. The use of second instead of the third harmonic exhibit strong experimental advantages. The most common set-up for phase control experiments [33] one comes across in the literature, involving third harmonic field, consists of three cells separated by LiF windows to allow transmission of the VUV third harmonic radiation. In the first cell third-harmonic generation occurs in Xe gas at focused laser geometries. The second cell serves as a

.

variable phase shifter utilizing the pressure dependence of the refractive index of the gas it is filled with, to produce an optical path delay between the electromagnetic fields. The mirror assembly shown in figure (5.2) creates parallel beams upon reflection from the first mirror and allows for achromatic focusing of both the fundamental and third-harmonic beam in the third cell, where the interference interaction takes place. A VUV monochromator is connected via a LiF window to the exit of the third cell in order to monitor the third-harmonic signal.

Comparing to the set up we used in our experiments, a major advantage in using second harmonic concerns the production process. Indeed the second harmonic generation with a BBO crystal is proved much more convenient to handle, the phase matching condition is met simply by tilting the crystal axis in respect to the incidence beam while in third harmonic accurate control of the gas pressure is needed. Additionally the conversion efficiency of the BBO crystal is high enough (~10%) providing a stabile beam of high intensity. On the other hand the use of third harmonic field posses difficulties concerning its propagation in several media, like air and common quartz optics. Therefore the retardation mechanism of its phase relative to that of the fundamental cannot be adjusted using common optics but techniques like the gas phase shifter must be employed. For these reasons the experimental procedure described in this work provides a robust solution of phase control experiments and is expected to provide increased stability and controlled reproducibility.

.
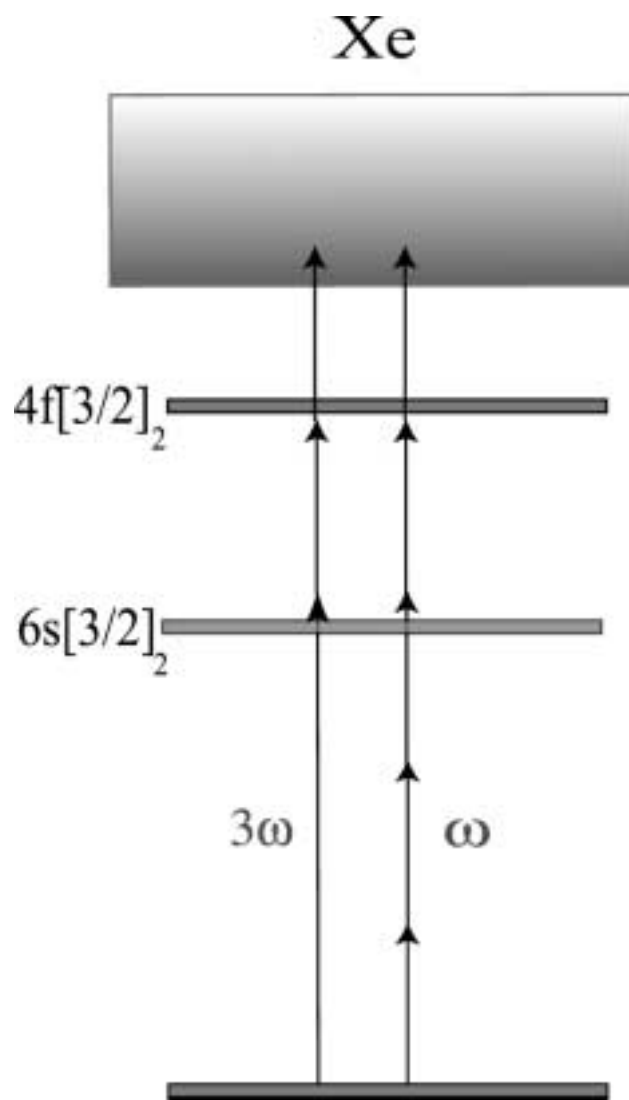
Fig5.1 3-photon resonance, five-photon multiphoton ionisation scheme used in Xe [32].

.
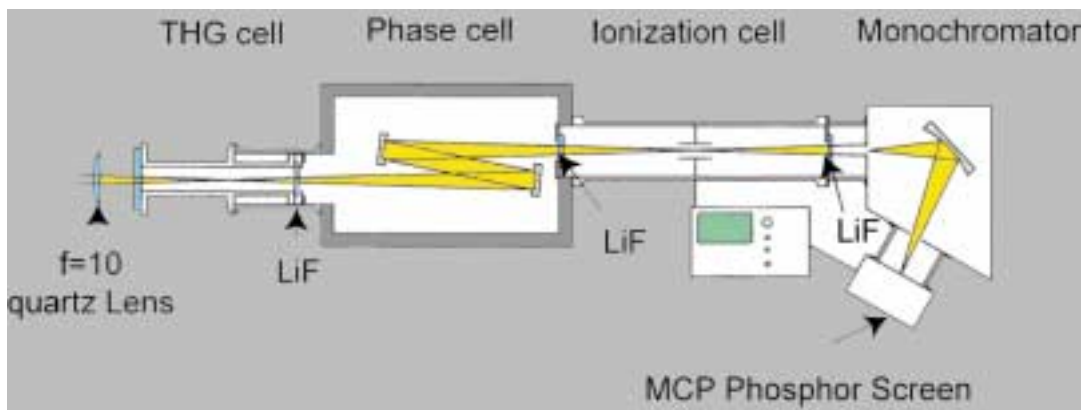
Fig5.2 Diagram of phase control experimental set up involving the third harmonic of the fundamental laser field.

.

5.2   On the control of AIS

As briefly mentioned in the introduction, it occurs from theoretical calculations [11-12] that in the presence of the two color laser field under consideration in experiment 2 the profile of the AIS is expected to be a function of the relative phase as well as of the intensity of the laser fields. It is predicted also that for a specific relation of the amplitudes of the interfering channels and specific relative phases the discrete or the continuum part of the AIS resonance can be canceled or enhanced. This can be understood in terms of the asymmetry of the resonance line shape modulating between symmetric, Lorenz like pattern, indicating a dominant contribution from the discrete part, and asymmetric pattern resulting from the continuum contribution which is usually a slowly varying function of the final state energy. On the measured spectra of the 2-photon (figure 4.2) and the 4-photon resonance (figure 4.5) as well as on the calculated cross section values (figures 4.3 and 4.4) the careful reader should note that apart from the asymmetry due to configuration interaction the resonance line shapes are strongly affected by intermediate resonances that

.

effect the virtual states in the multi photon excitation. The 4-photon resonance measured in our experiment has not been reported before in the literature and is in agreement with the calculated cross section as far as the resonance width, position and peak height are concerned.

As described in Appendix B the wave function and the line shape of an AIS can be understood in terms of diagonalizing the portion of the energy matrix that belongs to the subset of states $|\varphi\rangle$ and $\psi_{E'}$ of the coupled zero order eigenstates belonging to the discrete and the continuum manifolds respectively. In the high intensity regime the coupling of the ground state $|g\rangle$ to $|\varphi\rangle$ and $\psi_{E'}$ (see Appendix B for definitions) is strong enough (and perhaps to intermediate close resonances as well), therefore in this intensity regime diagonalization of the energy matrix subset is extended to include $|g\rangle$ (and possibly intermediate resonances) as well. The non diagonal matrix elements are affected by the interfering channels and are therefore dependent on the relative phase of the fileds. In a simplified manner this can be described that the 4+2 schemes that couple $|g\rangle$ to $|\varphi\rangle$ and $|g\rangle$ to $\psi_{E'}$ are in general different and this results in a phase dependence of the excitation and decay of the AIS (see figure 2.2) which translates in a phase dependence of the resonance line shape.

Involving the measurement of the relative phase (figure 4.6) it is evident that the resulting SHG signal modulation exhibit the expected periodicity in proportion to the ionisation signal as it occurs from the analysis in Appendix C. One has to

.

acknowledge that the absolute measurement of the relative phase is no trivial task since the propagation of the laser field through a number of optics to the interaction region exhibits dispersion effects that are generally frequency dependent and the effect of which cannot be measured in a straight forward manner. Therefore the measurements in figure (4.6) consist of a first approach to the problem of the relative phase measurement and involve an uncertainty of an initial phase θ_0 as a function of the fundamental wavelength.

Nevertheless one can be conclusive about the strong enhancement of the modulation depth localized (figure 4.8) around the position of the AIS resonance. This gives a strong evidence of the line shape phase dependence without though revealing the actual line shape of the resonance at various phases. Further interpretation of these results is in progress involving cross check with theoretical calculations [28] treating the initial phase θ_0 as a free parameter. Results from the later interpretation were not available at the time this essay was composed.

One way of measuring the relative phase exactly on the interaction region is possible if the angular distribution of the photoelectrons [34-37] produced in the ionisation is known at different relative phases. The requirements of such a measurement though consist far more than simple modifications on our experimental set up and are therefore not included in this work.

.

5.3   On the application to Xe

The measurements in experiment 3 obviously do not imply the presence of non zero phase lag between the two decay channels to $P_{3/2}$ and $P_{1/2}$ thresholds of Xe. This by no means supports the failure of theoretical predictions [12] since the scheme proposed in the later reference differs in the combination of photons used as well as in the final state energy, with all the implications that these come together. In our experiment the virtual state reached via four photon absorption is strongly enhanced by the close $4f[3/2]_2$ bound state, giving rice to the total cross section of the excitation, which is favorable in terms of higher signal to noise ratios in the measurements. On the other hand the case where the scheme becomes exactly resonant with the bound state would result in complete loss of coherence between the interfering channels connecting the ground atomic state to the final state in the continuum. As soon as the bound state gets populated, any information of the phase of the excitation channel is lost, in other words the excited electron 'forgets its past' and is further described by a single eigenstate

.

wave function of the atom. In experiment 3 the excitation scheme was investigated for several photon energies, including as large detuning from the $4f[3/2]_2$ resonance as the detection system allowed. Even though, the preservation of coherence in the interference on the final continuum state cannot be guaranteed, which is lethal for what the theoretical calculations predict [12]. Even in this case of decoherence, quantum interference would still occur between the ground state and the bound $4f[3/2]_2$ state. The observed decays to $P_{3/2}$ and $P_{1/2}$ thresholds would then result from the probe of the $4f[3/2]_2$ population to the continuum via one photon absorption. Therefore the photoelectron yields would modulate on phase and would depend only on the population transferred to the bound resonance. Due to the large number of photons involved in the excitation there are also channels that do not take part in the interference since they reach different final states, states of higher angular momentum in the continuum. For example the five photon transition (figure 5.1) can result in a $\Delta J=+5$ change of angular momentum but there is no other channel involving second harmonic photons that results in the same final state within the dipole approximation. These channels do not take part in the quantum interference and are known as *incoherent channels*. The presence of incoherent channels results in background contributions to the signals associated with the decays to $P_{3/2}$ and $P_{1/2}$ thresholds since the corresponding emitted photoelectrons have the same kinetic energies. Consider quantities A and B that are sinusoidal functions of the phase θ such that:

77

.

$$A = a \cdot \cos(\theta) \qquad\qquad (5.1a)$$

$$B = b \cdot \cos(\theta) \qquad\qquad (5.1b)$$

The value of the ratio A/B is obviously not phase dependent. If two different offsets D and C are added to the nominator and to the denominator of the ratio respectively then the quantity:

$$\frac{A+C}{B+D} = \frac{a \cdot \cos(\theta)+C}{b \cdot \cos(\theta)+D} \qquad\qquad (5.2)$$

Becomes phase dependent except in the special case where:

$$\frac{C}{a} = \frac{D}{b} \qquad\qquad (5.3)$$

where the cosine terms cancel.

Connecting to the previous discussion about the contribution from incoherent channels, we conclude that the later can result in a phase dependence of the ration of the decay signals to $P_{3/2}$ and $P_{1/2}$ thresholds in the general case. This

.

consisted of one of our main expectations for a method of controlling of the

decay ratio utilizing phase dependent coherent control.
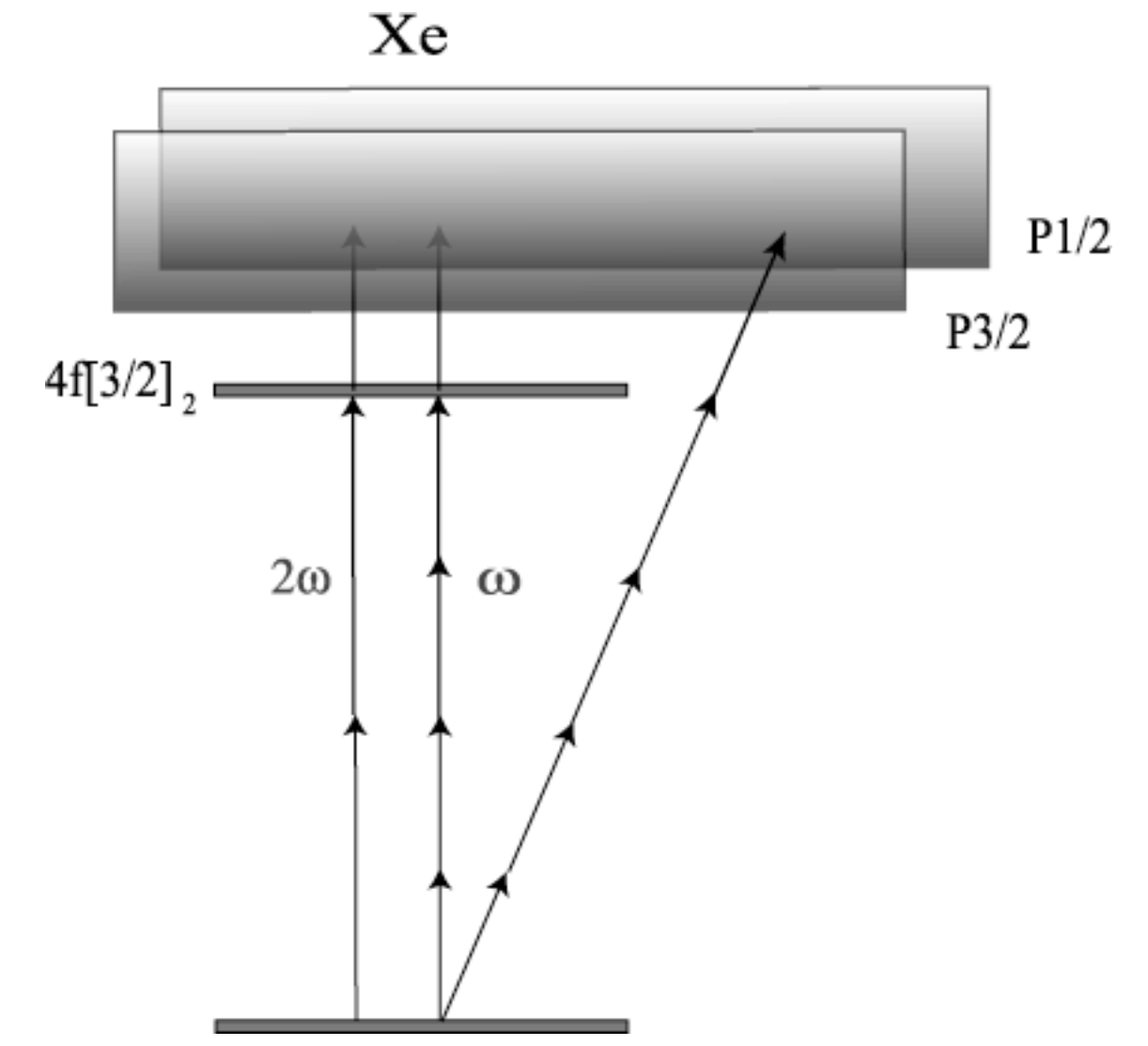
Fig. 5.3   Contribution to the photoelectron yield from incoherent channels. In the above scheme an incoherent channel is depicted which results in a change of angular momentum $\Delta l=+4$ and therefore does not take part in the quantum interference.

.

6.Conclusions

.

6.   Conclusions

In the present work we demonstrated a simple experimental procedure for phase-sensitive coherent control experiments, utilizing the second harmonic laser filed in two different set up variations, on-axis and Mach Zender like configurations. By applying this procedure we were able to obtain well reproducible phase-sensitive control of the ionization rates in xenon with high efficiency and under straightforward experimental conditions. Several advantages of the set up were discussed in comparison to 'traditional' phase control experiments using third harmonic field. The idea of using second harmonic laser field in such experiments was applied to more complicated control schemes involving excitation to multiple atomic continua and to autoionizing resonances. In the excitation above the $P_{3/2}$ and $P_{1/2}$ thresholds of Xe no phase lag was reported, and the possibilities of phase control of the decay ratio was discussed. The concept of controlling the excitation of an AIS and the Fano profile of the autoionizing resonance was further investigated experimentally. The measurements obtained showed strong enhancement of the modulation depth of the excitation rate localized in the vicinity of the $3p^2$ ^1S

81

.

state of Mg. Phase dependence as well as intensity effects in the control of the

AIS excitation were further discussed.

Appendixes

.

Appendix A   -   The Brumer-Shapiro scheme

Although several interference schemes are met in the coherent control literature for the purpose of presenting the basic formulation of the method we consider the case of interference between one- and three-photon pathways between a specified initial bound state and a specific product states in the continuum, as initially introduced by P. Brumer and M. Shapiro.

Let H_g and H_e be the Hamiltonians for the ground and excited states of a molecule, respectively. The initial state is taken to be an eigenstate of H_g with energy E_i, and the final state is in the continuum with energy E. Suppose the system, initially in its ground state, is irradiated with two electromagnetic fields:

$$E(t) = E_1 \cos(\omega_1 t + k_1 \cdot R + \theta_1) + E_3 \cos(\omega_3 t + k_3 \cdot R + \theta_3)$$ (A.1)

We consider the case when $\omega_3 = 3\omega_1$. In Equation (A.1), $E_a = |E_a|\varepsilon_a$, a =1,3 with $|E_a|$ the amplitude and ε_a the polarization unit vector of the incident field. Let $k_3 = 3k_1$, corresponding to parallel incident fields. The probability of forming a product in channel q with energy E is

.

$$W(E, q; E_i) = W_3(E, q; E_i) + W_1(E, q; E_i) + W_{13}(E, q; E_i) \qquad \text{(A.2)}$$

with $W_\alpha(E, q; E_i)$, $\alpha = 3, 1$ the transition probabilities corresponding to one-and three-photon absorption, respectively, and $W_{13}(E, q; E_i)$ the interference term between the one- and three-photon channels. In the weak field limit, the branching ratio for formation of products in exit channels q and q' is given by:

$$R_{qq'} = \frac{|E_3|^2 F_3^{(q)} - 2|E_3||E_1|^3 \cos\left(\theta_3 - 3\theta_1 + \delta_{13}^{(q)}\right)\left|F_{13}^{(q)}\right| + |E_1|^6 F_1^{(q)}}{|E_3|^2 F_3^{(q')} - 2|E_3||E_1|^3 \cos\left(\theta_3 - 3\theta_1 + \delta_{13}^{(q')}\right)\left|F_{13}^{(q')}\right| + |E_1|^6 F_1^{(q')}} \qquad \text{(A.3)}$$

where

$$F_3^{(q)} = \left(\frac{\hbar}{\pi|E_3|}\right)^2 W_3(E, q; E_i), \quad F_1^{(q)} = \left(\frac{\hbar}{\pi|E_1|^3}\right)^2 W_1(E, q; E_i) \qquad \text{(A.4)}$$

and similarly for q'. Both the numerator and denominator of Equation (A.3) obtain a sum of contributions from the independent one- and three-photon channels and a interference term. This term can be altered by changing the relative phase of the one- and three-photon channels, $(\theta_3 - 3\theta_1)$, and their relative amplitudes. Consequently the product ratio $R_{qq'}$ can be controlled. Calculations for a number of different molecular systems [29] demonstrate that, in principle, the ratio of the amounts of products in a branching reaction can be controlled

.

over a considerable range by varying the intensities and relative polarization of the one- and three-photon channels.

Appendix B – Wave function of the autoionizing state a' la Fano

Consider an atomic system with a number of zero approximation states, and among these one $|\varphi\rangle$ belonging to a discrete configuration and a continuum of states. We wish to diagonalize the portion of the energy matrix that belongs to the subset of states $|\varphi\rangle$ and $\psi_{E'}$. The elements of the sub matrix are indicated:

$$\langle\varphi|H|\varphi\rangle = E_{\varphi} \tag{B.1a}$$

$$\langle\psi_{E'}|H|\varphi\rangle = V_{E'} \tag{B.1b}$$

$$\langle\psi_{E''}|H|\psi_{E'}\rangle = E'\delta(E'' - E') \tag{B.1c}$$

A general solution for the form is assumed:

.

$$\Psi_E = a\varphi + \int dE' b_{E'} \psi_{E'} \tag{B.2}$$

the factors a and $b_{E'}$ are functions of E which is eigenvalue over the continuous

range of E'.

Under the above assumption the diagonalization reduces to the set of equations

for the coefficients a and $b_{E'}$:

$$E_\varphi a + \int dE' V_{E'}{}^* b_{E'} = Ea \tag{B.3a}$$

$$V_{E'} a + E' b_{E'} = E b_{E'} \tag{B.3b}$$

The solution follows the Dirac's procedure introducing the formal solution:

$$b_{E'} = \left[\frac{1}{E-E'} + z(E)\delta(E-E') \right] V_{E'} a \tag{B.4}$$

where the complex function $z(E)$ is to be determined later.

If the states $\psi_{E'}$ are represented by a wave function with asymptotic behaviour

$\propto \sin[k(E')r + \delta]$ then in the limit of large r the integral $\int dE' b_{E'} \psi_{E'}$ can be

expressed as:

.

$$\int dE' b_{E'} \psi_{E'} \propto \sin\left[k(E)r + \delta + \Delta\right] \tag{B.5}$$

where

$$\Delta = -\arctan\left[\pi / z(E)\right] \tag{B.6}$$

represents the *phase shift* due to configuration interaction of $\psi_{E'}$ with the state $|\varphi\rangle$. The values of z are determined by substituting expression (B.4) into (B.3a). The coefficient a factors out and will be determined later by the normalization condition.

$$E_\varphi + F(E) + z(E)|V_E|^2 = E \tag{B.7}$$

where

$$F(E) = P \int dE' \frac{|V_{E'}|^2}{E - E'} \tag{B.8}$$

P denotes the principal value of the integral. We have then:

$$z(E) = \frac{E - E_\varphi - F(E)}{|V_E|^2} \tag{B.9}$$

.

Notice that $|V_E|^2$ is an index of the strength of configuration interaction and has energy dimension. From equations (B.6) and (B.9) it occurs that the phase shift varies by $\sim\pi$ as E transverses an integral $\sim|V_E|^2$ about the resonance at $E = E_\varphi + F$. Therefore the quantity F represents a shift of the resonance position with respect to E_φ.

Proceeding with the normalization condition we come across the expression for coefficient α.

$$\langle \Psi_{\overline{E}} | \Psi_E \rangle = a^*(\overline{E})a(E) + \int dE' b_{E'}^*(\overline{E})b_{E'}(E) = \delta(E' - E) \qquad \text{(B.10)}$$

$$|a(E)|^2 = \frac{1}{|V_E|^2[\pi^2 + z^2(E)]} = \frac{|V_E|^2}{[E - E_\varphi - F(E)]^2 + \pi^2|V_E|^4} \qquad \text{(B.11)}$$

(Derivation of expression (B.11) involves some tedious algebra the presentation of which does not serve the purpose of this context.)

With reference to (B.6) and (B.4) we can finally write:

$$a = \sin\Delta / \pi V_E \qquad \text{(B.12a)}$$

.

$$b_{E'} = \frac{V_{E'}}{\pi \cdot V_E} \frac{\sin \Delta}{E - E'} - \cos \Delta \cdot \delta(E - E')$$ (B.12b)

$$\Delta = -\arctan \frac{\pi \cdot |V_E|^2}{E - E_\varphi - F(E)}$$ (B.12c)

Consider an excitation mechanism coupling an initial bound state $|i\rangle$ to the AIS defined above. The excitation probability is then expressed:

$$\langle \Psi_E |T| i \rangle = \frac{1}{\pi \cdot V_E^*} \langle \Phi |T| i \rangle \sin \Delta - \langle \psi_E |T| i \rangle \cos \Delta$$ (B.13)

where

$$\Phi = \varphi + P \int dE' \frac{V_{E'} \psi_{E'}}{E - E'}$$ (B.14)

indicates the state φ *modified by an admixture* of states of the continuum.

The sharp variation of Δ as it passes through the resonance at $E = E_\varphi + F$ causes a sharp variation of $\langle \Psi_E |T| i \rangle$. More spacifically, $\sin \Delta$ is an even function of $E - E_\varphi - F$,whereas $\cos \Delta$ is an odd function of this variable. Therefore the contributions to $\langle \Psi_E |T| i \rangle$ represented in (B.13) by from $\langle \Phi |T| i \rangle$ and $\langle \psi_E |T| i \rangle$ *interfere with opposite phase* on the two sides of the resonance. The

89
.

transition probability *vanishes* on one side of the resonance, at $\Delta = \Delta_0$ that is $E = E_0$ where:

$$\tan \Delta_0 = -\frac{E_0 - E_\varphi - F(E_0)}{\pi \cdot |V_{E_0}|^2} = \frac{\pi \cdot V_{E_0}{}^* \langle \psi_{E_0} | T | i \rangle}{\langle \Phi | T | i \rangle} \tag{B.15}$$

At this point we introduce the reduced energy variable defined by the following relation:

$$\varepsilon = -\cot \Delta = \frac{E - E_\varphi - F(E)}{\pi \cdot |V_E|^2} = \frac{E - E_\varphi - F}{\frac{1}{2}\Gamma} \tag{B.16}$$

in which

$$\Gamma = 2\pi \cdot |V_E|^2 \tag{B.17}$$

indicates the resonance width, while the quantities E_φ and F are approximated to have constant value over the resonance.

In this context the ratio of the transition probability to AIS over the transition probability to the smooth continuum can be written:

.

$$\frac{\left|\left\langle \Psi_E \left| T \right| i \right\rangle\right|^2}{\left|\left\langle \psi_E \left| T \right| i \right\rangle\right|^2} = \frac{(q+\varepsilon)^2}{1+\varepsilon^2} \qquad (B.18)$$

where the *q parameter* is defined as:

$$q = \frac{\left\langle \Phi \left| T \right| i \right\rangle}{\pi \cdot V_E^* \left\langle \psi_E \left| T \right| i \right\rangle} \qquad (B.19)$$

and is of grate experimental interest since the resonance line shape is fully described by this parameter. This conclusion is summarized in figure (B.1) where the resonance line shape is plotted for several values of the q parameter.
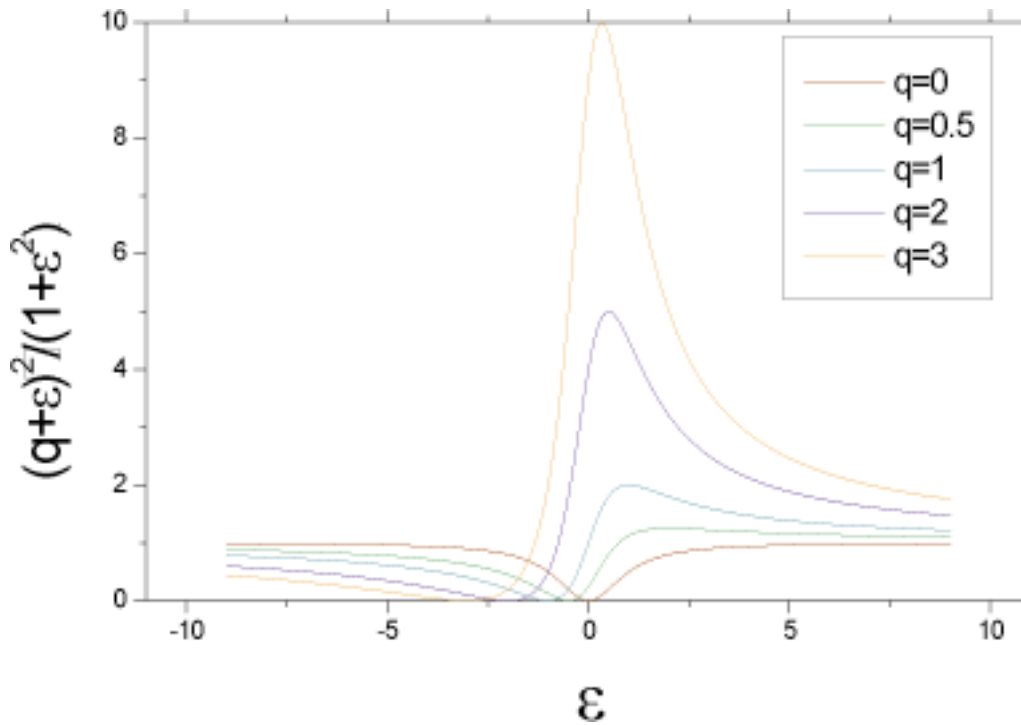
Fig B.1. Natural line shapes for different values of q.

.

Appendix C – Propagation of E.M. field in a second order non linear medium

In the case of a nonlinear medium with non second order susceptibility the induced polarization can be expressed as sum of a linear an a nonlinear term:

$$D = \varepsilon E + P_{NL} \qquad (C.1)$$

The nonlinear term in the case of a SHG crystal is given by

$$P_{NL}^{(2\omega)}(z,t) = \chi^{(2\omega)}[E(z,t)]^2 \qquad (C.2)$$

Where $E(z,t)$ is the driving field and $\chi^{(2\omega)}$ is the second order nonlinear susceptibility of the medium. The propagation in this medium is described by:

$$\nabla^2 E = +\mu_0 \varepsilon \frac{\partial^2 E}{\partial t^2} + \mu_0 \frac{\partial^2 P_{NL}}{\partial t^2} \qquad (C.3)$$

.

upon substitution of analytic expressions for the two colour fields the later equation becomes:

$$E^{(\omega)}(z,t) = \left[E_0^{(\omega)}(z,t) e^{i(\omega t - kz)} + c.c \right] \hat{z} \qquad (C.4)$$

$$P_{NL}^{(2\omega)}(z,t) = \left[P_0^{(2\omega)}(z,t) e^{i(2\omega t - 2kz)} + c.c \right] z \qquad (C.5)$$

$$-2ik_{2\omega} \frac{\partial \vec{E}_{(z,t)}^{(2\omega)}}{\partial z} + k_{2\omega}^2 E_0^{(2\omega)}(z,t) - 4\mu_0 \varepsilon \omega^2 E_0^{(2\omega)}(z,t) - 4i\mu_0 \varepsilon \omega \frac{\partial \vec{E}_{(z,t)}^{(2\omega)}}{\partial t} =$$
$$-4\mu_0 \omega^2 P_0^{(2\omega)}(z,t) e^{i\Delta kz}$$

$$(C.6)$$

where $\Delta k = 2k - k_{2\omega}$ is the relative phase of the two fields.

To simplify the above expression one makes the slowly varying amplitude approximation in space and in time domain:

$$\left| \frac{\partial^2 E_{(z,t)}^{(2\omega)}}{\partial z^2} \right| << k \left| \frac{\partial E_{(z,t)}^{(2\omega)}}{\partial z} \right| \qquad (C.7)$$

.

$$\left| \frac{\partial^2 E_{(z,t)}^{(2\omega)}}{\partial t^2} \right| << 4i\omega \left| \frac{\partial E_{(z,t)}^{(2\omega)}}{\partial t} \right|$$

(C.8)

Thus the wave equation becomes:

$$\frac{\partial \vec{E}_{(z,t)}^{(2\omega)}}{\partial z} + \frac{1}{u}\frac{\partial \vec{E}_{(z,t)}^{(2\omega)}}{\partial t} = -\frac{i(2\omega)}{2c\varepsilon_0 n} \ P_0^{(2\omega)}(z,t)e^{i\Delta kz}$$

(C.9)

where u=c/n is the speed of light in the medium for the 2ω field. The left hand side of the equation describes the propagation of the harmonic field inside the medium while the right hand side describes the driving polarization (as a function of position and time).

The –*i* factor of the above expression is the origin of the phase difference of π/2 between the fundamental and the harmonic field mentioned before. While the phase matching condition insures the maximum energy conversion into the harmonic field.

$$\Delta k = 2k - k_{2\omega} = 0$$

(C.10)

94

.

Deviation from the above condition results in a periodic exchange of energy between the harmonic field and the medium throughout the propagation and therefore in lower efficiency in the harmonic generation.

.

Appendix D – Transition Rate calculations

Consider atoms exposed to strong electromagnetic field which undergo multi photon ionization (MPI). According to lowest-order perturbation theory (LOPT) the rate $\frac{dP}{dt}(\sec^{-1})$ of an *N*-photon process is:

$$\frac{dP}{dt}(t) = [1 - P(t)] \cdot \sigma^{(N)} \Phi^N(t) \tag{D.1}$$

where $P(t)$ is the probability of finding the atom ionized at time t, $\sigma^{(N)}$ is the generalized *N*-photon cross section (in $cm^{2N} \sec^{N-1}$) and $\Phi(t)$ is the photon flux as a function of time (in $cm^{-2} \sec^{-1}$).

Our case of interest is ionization from intense laser pulses, therefore from eq. (D.1) the evolution of the ionization probability is derived [30] [31].

$$P(t) = 1 - \exp\left(- \int_{-\infty}^{t} \sigma^{(N)} \Phi^N(t') dt' \right) \tag{D.2}$$

.

The maximum photon flux is denoted Φ_0 and then $F(t)$ is the laser pulse temporal profile normalized at the peak intensity, then one can write:

$$\Phi(t) = \Phi_0 \cdot F(t) \tag{D.3}$$

$$t_{eff} \equiv \int_{-\infty}^{+\infty} F^N(t')dt' \tag{D.4}$$

Equation (D.4) defines the effective pulse duration.

The asymptotic behavior of the ionization probability, after the pulse is completed (so for $t \to \infty$) is given:

$$P(t \to \infty) = 1 - \exp\left(-\sigma^{(N)} \cdot \Phi_0^N \cdot t_{eff}\right) \tag{D.5}$$

The saturation intensity is defined by:

$$\sigma^{(N)} \cdot \Phi_0^N \cdot t_{eff} = 1 \tag{D.6}$$

$$\boxed{I_{sat} = \hbar\omega\left(\sigma^{(N)} \cdot t_{eff}\right)^{-\frac{1}{N}}} \tag{D.7}$$

.

References

.

References

1. Tannor DJ, Rice SA. *Adv. Chem. Phys.* **70** 441 (1988)

2. Baumert T, Gerber G. *Isr. J. Chem.* **34** 103 (1994)

3. Brumer P, Shapiro M. *Acc. Chem. Res.* **22** 407 (1989).

4. Chen Ce and Elliott D S *Phys. Rev. Lett.* **65,** 1737 (1990)

5. M. Shapiro, J. W. Herburn, and P. Brumer, Chem. Phys. Lett. **149**, 451 (1988).

6. Chen Ce, Yi-Yian Yin, and D. Elliott, Phys. Rev. Lett. **64**, 507 (1990).

7. A. D. Bandrauk, J. M. Gauthier, and J. F. McCann, Chem. Phys. Lett. **200**, 399 (1992).

8. E. Charron, A. Giusti-Suzor, and F. H. Mies, Phys. Rev. Lett. **71**, 692 (1993).

9. Zhu LC, Kleiman V, Li XN, Lu S-P, Trentelman K, Gordon RJ. *Science* **270**, 77 (1995).

10. Zhu L, Fiss J, Suto K, Wada R, Seideman T, Gordon RJ. *Phys. Rev. Lett.* **79**, 4108(1997)

11. T. Nakajima and P. Lambropoulos, Phys. Rev. Lett. **70**, 1081 (1993).

12. T. Nakajima and P. Lambropoulos, Phys. Rev. A **50**, 595 (1993).

13. E. Dupont, P. B. Corkum, Liu Hc, M. Buchanan, and Z. R. Wasilewski, Phys. Rev. Lett. **74**, 3596 (1995).

.

14. B. Sheehy, B. Walker, and L. F. DiMauro, Phys. Rev. Lett. **74**, 4799 (1995).

15. Langchi Zhu, V. Kleiman, Xiaonong Li, Shao-Ping Lu, K. Trentelman, Yongjin Xie, and R. J. Gordon, Science **270**,77 (1995).

16. Langchi Zhu, Kunihiro Suto, J. A. Fiss, R. Wada, T. Seide-man, and R. J. Gordon, Phys. Rev. Lett. **79**, 4108 (1997).

17. S. Cavalieri, R. Eramo and L. Fini, Phys. Rev. A **55**, 2941 (1997).

18. D. Xenakis, N. E. Karapanagioti, C. Fotakis, and D. Charalambidis, Opt. Commun. **152**,83 (1998).

19. Lambropoulos P, Nakajima T *Phys. Rev. Lett.* **82,** 2266 (1999)

20. Takashi Nakajima, Jian Zhang and P Lambropoulos *Journal of Physics* **30** 1077 (1997)

21. U. Fano *Phys. Rev.* **124**, 1866 (1961)

22. P. Lambropoulos and P. Zoller *Phys. Rev. A* **24**, 379 (1981)

23. Moccia, P. Spizzo *Phys. Rev. A* **39** 3855 (1989)

24. Y. L. Chao, K. Fotakis and D. Charalambidis *Phys. Rev. A* **48** 3636 (1993)

25. U. Fano *Phys. Rev.* **124,** 1866 (1961)

26. P. Lambropoulos and P. Zoller *Phys. Rev. A* **24**, 379 (1981)

27. Y. Shao, C. Fotakis and D. Charalambidis *Phys. Rev. A* **48**, 3636 (1993)

28. A. Saenz (private communication)

29. Chan CK, Brumer P, Shapiro M. *J. Chem. Phys.* **94**, 2688 (1991)

30. P. Lambropoulos, Comments *At. Mol. Phys*. **20**, 199 (1987)

31.   P. Lambropoulos and X. Tang *J. Op. Soc. Am. B* **4**, 821 (1987)

32.   N E Karapanagioti, D Xenakis, D Charalambidis and C Fotakis *J. Phys. B* **29,** 3599 (1996)

33.   Chen Ce and Elliott D S *Phys. Rev. Lett.* **65,** 1737 (1990)

34.   B. Sheehy, B. Walker and L.F DiMauro *Phys. Rev. Lett.* **74**, 4799 (1995)

35.   Yi- Yian Yin, Ce Chen and D. S. Elliot *Phys. Rev. Lett* **69**, 2353 (1992)

36.   D. W. Schumacher, F. Weihe, H. G. Muller and P. H. Bucksbaum *Phys. Rev. Lett* **73**, 1344 (1994)

37.   Yi- Yian Yin, D. S. Elliot, R. Shehadeh, E. R. Grant *Chem. Phys. Lett.* **241**, 591 (1995)

38.   Giacinto Scoles *Atomic and Molecular Beam Methods* Oxford University Press, New York (1988)